ISSN 2812-9474

Engineering TODAY

VOL. 1 / NO. 2 / 2022

PUBLISHED BY

The Faculty of Mechanical and Civil Engineering
in Kraljevo of the University of Kragujevac

ISSN 2812-9474

VOL. 1 / NO. 2 / 2022

ET

Engineering TODAY

PUBLISHED BY

The Faculty of Mechanical and Civil Engineering
in Kraljevo of the University of Kragujevac

Engineering TODAY

PUBLISHER

The Faculty of Mechanical and Civil Engineering in Kraljevo of the University of Kragujevac

ADDRESS

Faculty of Mechanical and Civil Engineering
Dositejeva 19, 36000 Kraljevo
Republic of Serbia

CONTACT

Tel: +381 36 383 269
+381 36 383 377
+381 36 383 378

Fax: +381 36 383 269

Email: editor@engineering-today.com

Web: www.engineering-today.com

FREQUENCY

4 issues per year

PRINTED BY

Grafika Galeb d.o.o, Niš

CIRCULATION

50 copies/issue

INSTRUCTION FOR AUTHORS

A Engineering TODAY manuscript should by written clearly and concisely in correct English. The length of a reviewing paper is up to 12 pages. All papers are subject to a reviewing process. Final acceptance of a paper for publication in the Journal is based on the decision of the Editorial Board.

TEMPLATE FOR MANUSCRIPT

Template can be downloaded from the journal's website.

SUBMISSION OF PAPERS

All manuscripts for consideration by the Engineering TODAY should be submitted via the journal's website.

CIP - Каталогизација у публикацији
Народна библиотека Србије, Београд

621(497.11)

ENGINEERING Today / editor in chief Radovan Bulatović. - Vol. 1, No. 2 (2022) - . - Kraljevo : The Faculty of Mechanical and Civil Engineering, University of Kragujevac, 2022 - (Niš : Grafika Galeb). - 30 cm

Tromesečno. - Je nastavak: IMK-14 = ISSN 0354-6829. -
Drugo izdanje na drugom medijumu:
Engineering Today (Kraljevo. Online) = ISSN 2812-9938
ISSN 2812-9474 = Engineering Today (Kraljevo)
COBISS.SR-ID 64530953

PROOFREADERS

TECHNICAL EDITORS

AIMS AND SCOPE

Engineering Today is an international peer-reviewed scientific journal that publishes original papers, both theoretical and experimental, covering the whole spectrum of engineering sciences, but focusing mostly on mechanical, electrical and civil engineering. The primary objective is to provide a high-level platform for researchers and practitioners to disseminate theoretical or engineering-oriented research output achievements within the context of engineering systems that fosters knowledge sharing in different branches of engineering discipline.

Engineering Today also publishes novel theoretical methods, algorithms, simulations, experiments, and case studies as applications of state-of-the-art research in the field of engineering.

The topics of interest include, but are not limited to:

- Mechanical engineering
- Electrical/electronic engineering
- Civil engineering
- Manufacturing engineering
- Software engineering
- Thermal technique and environment protection
- Applied mathematics and physics
- Theoretical and applied mechanics
- Optimization algorithms
- Metaheuristic algorithms
- Railway engineering
- Earth-moving, construction and transportation machinery
- Automatic control and fluid technique
- Computer science
- Information systems
- Fault detection and diagnosis
- Learning systems
- Robust systems
- Neuro-fuzzy systems
- Internet of things
- Cybernetics
- System identification
- Stochastic systems
- Complex networks
- Computational complexity
- Mechatronics
- Production technologies
- Computer design and computer integrated processes design
- Design of machining processes
- Engineering management and entrepreneurship
- Mechanical construction and material technology
- Interdisciplinary applications

It provides an effective medium for researchers and a way to quickly publish high-quality original papers, so as to convey the latest important progress in their professional field to scientists in related disciplines. Engineering Today offers authors rigorous peer review, rapid publication, and maximum visibility. The journal expects to accept only the most relevant manuscripts and will provide very rapid evaluation to prevent publication delays. The Editors reserve the right to reject papers without sending them out for review.

From time to time, Engineering Today will publish review articles, short communications, discussions as well as special issues on a specific sub-field of engineering science. Authors are encouraged to contact the Editor-in-Chief if they would like to submit a review article or propose and edit a special issue of the journal.

Engineering
TODAY

VOL. 1 / NO. 2 / 2022

CONTENTS

ORIGINAL SCIENTIFIC PAPER OPEN ACCESS

Thermal stability of lubricants in cycloidal reducers

Milan Vasić[1*], Mirko Blagojević[2], Mircea V. Dragoi[3]

[1] The Academy of Applied Technical Studies Belgrade, The College of Applied Engineering Sciences in Pozarevac, Serbia

[2] University of Kragujevac, Faculty of Engineering, Kragujevac, Serbia

[3] Transilvania University of Brasov, Manufacturing Engineering Department, Brasov, Romania

ARTICLE INFO

[*] **Correspondence:** milan.vasic@vts-pozarevac.edu.rs

DOI: 10.5937/engtoday2202007V

UDC: 621(497.11) **ISSN:** 2812-9474

Article history: Received 02 June 2022; Accepted 20 June 2022

ABSTRACT

There is intensive rolling and sliding between the meshing elements of a cycloidal reducer, whereby a significant amount of mechanical energy is converted into heat and absorbed by the lubricant. In order to stabilize the temperature of the lubricant, it is necessary to achieve thermal equilibrium, i.e. the amount of heat dissipated should equal the amount of heat generated. A complex task of determining the equilibrium temperature of a lubricant generally involves theoretical analysis, numerical calculation, computational simulations and experimental testing.

The aim of this paper is to develop a model to predict the amount of heat dissipated from the outer surface of the housing as well as the equilibrium temperature of the lubricant. The model is based on the basic laws of thermodynamics, while the computational simulation is performed for an actual cycloidal reducer in the Matlab software package. The simulation results show changes in the equilibrium temperature in relation to: the coefficient of heat transfer from the lubricant to the inner wall of the housing, ambient air velocity, wall thickness and housing material.

KEYWORDS

Cycloidal reducer, Heat generation, Heat dissipation, Thermal equilibrium, Thermal stability of lubricants

1. INTRODUCTION

Compared to other speed reducers, cycloidal reducers cover a wide range of gear ratios, have high efficiency, compact construction, light weight, low noise and low vibration. Thermal stability, which plays a crucial role in maintaining the proper functioning and intended use of cycloidal reducers, mainly depends on the lubricant used and the housing design.Inside the housing, there is intensive rolling and sliding between the meshing elements, whereby a significant amount of mechanical energy is converted into heat and absorbed by the lubricant. An increase in the temperature of the outer surface of the housing and the lubricant in relation to the ambient temperature indicates excessive heating. In order to stabilize the temperature of the lubricant, it is necessary to achieve thermal equilibrium, i.e. the amount of heat dissipated should equal the amount of heat generated.

There is currently little research on thermal behaviour of cycloidal reducers. Zah et al. [1] used an equilibrium equation, i.e. they equalled the amount of heat generated and the amount of heat dissipated in order to determine the operating temperature of the housing. Kudryavcev's model was used to predict the amount of mechanical energy converted into heat [2]. Nowadays, after years of research, other models based on a larger number of contacts between the elements are available [3-6]. Mihailidis et al. [7-8] used thermal elastohydrodynamic lubrication theory to determine the contact area temperatures independently of power losses. Wei et al. [9] investigated distribution of the temperature field on one tooth of a cycloidal reducer, assuming that the load and the heat transfer are the same for all the teeth. Olejarczyk et al. [10] investigated operating temperatures of mineral and synthetic oils. A lot of researchers studied thermal stability of worm gears [11-13]. Xue and Xu [14] investigated the heat transfer mechanism of each element in a cylindrical helical gearbox. Zivkovic [15] studied planetary gearbox and established a relation between mechanical losses and the amount of heat dissipated to the ambient air.

Based on the review of the literature, it can be concluded that the lubricant operating temperature has a crucial impact on the thermal stability of a gearbox. Optimal lubrication can be ensured only within the right range of operating temperature. Therefore, the aim of this paper is to define a simplified theoretical model to predict the operating temperature of the lubricant and the amount of heat dissipated only through the housing.

2. ENERGY BALANCE IN THE CYCLOIDAL REDUCER

In order to establish the thermal stability and to determine the operating temperature of the lubricant in the cycloidal reducer, it is necessary to define the place and the manner, i.e. the elements on which the mechanical energy is converted into heat and the way the heat is dissipated.

In general, the contacts between the elements of a cycloidal reducer can be divided into load-independent and load-dependent contacts [6,16]. Apart from the housing parts, the load-independent contacts are mainly related to the lubricant and the shaft sealing elements. Load-dependent contacts can be divided into the contacts:

- in the cycloid disc bearing;
- between the output rollers and holes in the cycloid disc;
- between the output rollers and their pins;
- between the ring gear rollers and the cycloid disc teeth;
- between the ring gear rollers and their pins;
- in the input shaft bearings;
- in the output shaft bearings.

The entire mechanical energy converted into heat during these contacts is absorbed by the lubricant and transferred by convection to all internal parts, including the inner surface of the housing. The heat is dissipated to the ambient air through a relatively large outer surface of the housing, through the housing foot, but also through free parts of the shaft, regardless of their relatively small surface areas. Table 1 shows the predominant ways of heat transfer between the cycloidal reducer elements.

Table 1: The ways of heat transfer in the cycloidal reducer

Heat transfer	The predominant mode of heat transfer
Conduction	All internal elements in contact with each other
Convection	All internal elements in contact → lubricant
	Lubricant → air in the gearbox
	Housing → ambient air
	Housing foot → ambient air
	Input/output shaft → ambient air
	Input/output shaft coupling → ambient air
Radiation	Housing → ambient air
	Housing foot → ambient air
	Input/output shaft → ambient air
	Input/output shaft coupling → ambient air

Since a simplified model is used, when determining the equilibrium temperature of the lubricant, the heat dissipated through the housing foot and as well as through the input and output shaft of the cycloidal reducer is neglected.

3. EFFICIENCY OF THE CYCLOIDAL REDUCER

As a result of many years of research, numerous models are available to predict the efficiency of cycloidal reducers. One of the most commonly used models was defined by Malhotra [3]. It is rather simple, easy to use and it gives good results. The total efficiency is determined based on the following expression:

$$\eta = \frac{T_{in} \cdot 2\pi - W_f}{T_{in} \cdot 2\pi} \tag{1}$$

where: T_{in} – input shaft torque; W_f – total work done by the friction force.

The total work done by the friction force (W_f) is the integral of the sum of elementary work: friction in the bearing of cycloid disc, rolling friction between the output rollers and the holes in the cycloid disc, rolling friction between the cycloid discs and the ring gear rollers, sliding friction between the output rollers and their pins, as well as sliding friction between the ring gear rollers and their pins. The comprehensive expression can be written in the following form [6]:

$$\begin{aligned} W_f = {} & \frac{f_{r1} \cdot D_{SR} \cdot z_1}{d_{kt}} \int_0^{\frac{2\pi}{z_1}} F_E(\beta) \cdot d\beta + z_1 \cdot \left(f_{r2} + \frac{\mu_{s1} \cdot d_{VK}}{2} \right) \cdot \int_0^{\frac{2\pi}{z_1}} \sum_{j=1}^{q} F_{Kj}(\beta) \cdot d\beta + \\ & + (z_1 + 1) \cdot \left(f_{r3} + \frac{\mu_{s2} \cdot d_0}{2} \right) \cdot \int_0^{\frac{2\pi}{z_1}} \sum_{i=1}^{p} F_{Ni}(\beta) \cdot d\beta \end{aligned} \tag{2}$$

where: f_{r1} – lever arm of the rolling friction of the cycloid disc $(f_{r1} = \mu_{r1} \cdot d_{kt} / 2)$; μ_{r1} – coefficient of rolling friction in the cycloid disc bearing; $F_E(\beta)$ – current value of the eccentric cam force; D_{SR} – mean diameter of the cycloid disc bearing $(D_{SR} = (D_{CZ} + d_{CZ}) / 2)$; D_{CZ} – outer diameter of the cycloid disk bearing; f_{r2} – lever arm of the rolling friction of the output roller $(f_{r2} = \mu_{r2} \cdot D_{VK} / 2)$; μ_{r2} – coefficient of rolling friction between the output rollers and the hole in the cycloid disc; $F_{Kj}(\beta)$ – current value of the output force on the *j-th* output roller; q – current number of the output rollers participating in the load transfer (if the total number of output rollers (u) is even, then $(q = u / 2)$, if it is an odd number, then $(q = (u-1)/2)$); f_{r3} – lever arm of the rolling friction of the ring gear rollers $(f_{r3} = \mu_{r3} \cdot D_0 / 2)$; μ_{r3} – coefficient of the friction between the ring gear rollers and the cycloid disc; $F_{Ni}(\beta)$ – current value of the normal force on the *i-th* ring gear roller; p – current number of ring gear rollers participating in the load transfer. If the total number of the ring gear rollers is even, then $(p = z_2 / 2)$, and if it is an odd number, then $(p = (z_2 + 1)/2)$.

4. THE QUANTITY OF DISSIPATED HEAT

Defining a mathematical model for the amount of heat dissipated through the housing wall is very complex due to the specific geometry of the housing. Therefore, a simplified model (Figure 1) is used with the following approximations:

- the housing is homogeneous and isotropic with flat vertical and cylindrical horizontal surfaces;
- the inside surface of the housing is in contact only with a constant-temperature lubricant.

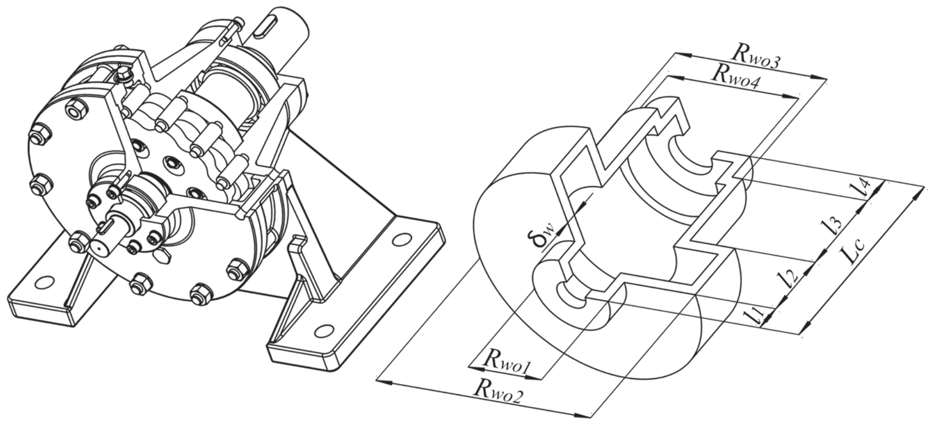

Figure 1: Simplified housing model for thermal analysis

4.1 The amount of heat dissipated through the flat wall of the housing

For the one-dimensional heat flow through the flat wall (Q_{hf}), which receives heat from the lubricant by convection on the inside and transfers heat to the ambient air by convection and radiation on the outside (Figure 2), the following equations can be written [17-18]:

$$Q_{hf} = \alpha_{lub} \cdot A_{wi,f} \cdot (t_{lub} - t_{wi,f}) = \frac{\lambda_w}{\delta_w} \cdot A_{we,f} \cdot (t_{wi,f} - t_{wo,f}) = (\alpha_{air,fcon} + \alpha_{air,rad}) \cdot A_{wo,f} \cdot (t_{wo,f} - t_{air}) \tag{3}$$

$$Q_{hf} = \frac{(t_{lub} - t_{wi,f})}{1/\alpha_{lub} \cdot A_{wi,f}} = \frac{(t_{wi,f} - t_{wo,f})}{\delta_w / \lambda_w \cdot A_{we,f}} = \frac{(t_{wo,f} - t_{air})}{1/(\alpha_{air,fcon} + \alpha_{air,rad}) \cdot A_{wo,f}} \tag{4}$$

$$Q_{hf} = \frac{(t_{lub} - t_{wi,f})}{R_{f,lub}} = \frac{(t_{wi,f} - t_{wo,f})}{R_{f,wal}} = \frac{(t_{wo,f} - t_{air})}{R_{f,air}} \tag{5}$$

$$Q_{hf} = \frac{(t_{lub} - t_{air})}{R_{f,total}} \tag{6}$$

$$R_{f,total} = R_{f,lub} + R_{f,wal} + R_{f,air} \tag{7}$$

where: t_{lub} – lubricant temperature; $t_{wi,f}$ – temperature of the inner flat wall of the housing; $t_{wo,f}$ – temperature of the outer flat wall of the housing; t_{air} – ambient temperature; $A_{wi,f}$ – inner surface area of the flat wall of the housing; $A_{wo,f}$ – outer surface area of the flat wall of the housing; $A_{we,f}$ – equivalent surface area of the flat wall $(A_{we,f} = (A_{wi,f} + A_{wo,f})/2)$; α_{lub} – coefficient of heat transfer from the lubricant to the inner wall of the housing (according to Jelaski [19], the value of the coefficient (α_{lub}) ranges from $150 \div 300 W/(m^2K)$, but it is usually taken to be $\alpha_{lub} = 200 W/(m^2K)$ [20]); $\alpha_{air,fcon}$ – coefficient of convective heat transfer from the outer flat wall of the housing to the ambient air; $\alpha_{air,rad}$ – coefficient of heat transfer by radiation from the outer wall of the housing to the ambient air; λ_w – coefficient of thermal conductivity (for cast steel $\lambda_w = 50 W/mK$) [21]; δ_w – equivalent thickness of the vertical flat wall of the housing; $R_{f,lub}$ – thermal resistance to heat transfer from the lubricant to the inner wall; $R_{f,wal}$ – thermal resistance to heat transfer through the flat wall; $R_{f,air}$ – thermal resistance to heat transfer from the outer flat wall to the ambient air.

Since heat always flows from a higher to a lower temperature area in order to equalize the temperatures, it is assumed that $(t_{lub} > t_{air})$.

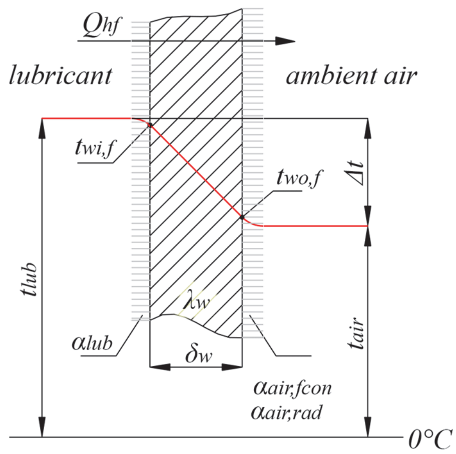

Figure 2: Heat dissipation through the vertical flat wall of the housing (Δt – the temperature difference between the lubricant and the ambient air)

If the outer surface temperature of the housing wall (t_{wo}) is known, Churchill and Chu [22-23] proposed the following correlation equations to determine the heat transfer coefficient $(\alpha_{air,fcon})$:

$$\alpha_{air,fcon} = \frac{N_{u,fo} \cdot \lambda_{air}}{H_{wo}} \tag{8}$$

$$N_{u,fo} = 0,68 + \frac{0,670 \cdot R_{a,fo}^{\ 1/4}}{\left[1 + \left(0,492 / P_{r,fo}\right)^{9/16}\right]^{4/9}} \qquad R_{a,fo} < 10^9 \tag{9}$$

$$N_{u,fo} = \left\{0,825 + \frac{0,387 \cdot R_{a,fo}^{\ 1/6}}{\left[1 + \left(0,492 / P_{r,fo}\right)^{9/16}\right]^{8/27}}\right\}^2 \qquad R_{a,fo} > 10^9 \tag{10}$$

$$R_{a,fo} = G_{r,fo} \cdot P_{r,fo} \tag{11}$$

$$R_{e,fo} = \frac{\rho_{air} \cdot \mathrm{w}_{air} \cdot H_{wo}}{\mu_{air}} = \frac{\mathrm{w}_{air} \cdot H_{wo}}{\nu_{air}} \tag{12}$$

$$P_{r,fo} = \frac{c_{p,air} \cdot \mu_{air}}{\lambda_{air}} \tag{13}$$

$$G_{r,fo} = \frac{\beta \cdot g \cdot H_{wo}^{\ 3} \cdot \left(t_{wo} - t_{air}\right)}{\nu_{air}^{\ 2}} \tag{14}$$

where: $N_{u,fo}$ – Nusselt number; $R_{e,fo}$ - Reynold number; $P_{r,fo}$ – Prandtl number; $G_{r,fo}$ – Grashof number. The ambient air parameters include: ρ_{air} – density; w_{air} – air velocity; μ_{air} – dynamic viscosity; ν_{air} – kinematic viscosity; $c_{p,air}$ – specific heat capacity at the constant pressure; λ_{air} – coefficient of thermal conductivity. The rest of the quantities are: H_{wo} – height of the outer flat wall; β – coefficient of thermal expansion $\left(\beta = 1/t_{ekv}\right)$; t_{ekv} – equivalent temperature $\left(t_{ekv} = \left(t_{wo,f} - t_{air}\right)/2\right)$, g – acceleration of gravity $\left(g = 9.81 m/s^2\right)$.

For practical calculations, an empirical expression which gives acceptable results can also be used [24]:

$$\alpha_{air,fcon} = 7 + 12 \cdot \sqrt{w_{air}} \tag{15}$$

The heat transfer coefficient $\left(\alpha_{air,rad}\right)$ can be determined based on the expression [18]:

$$\alpha_{air,rad} = \varepsilon \cdot \sigma \cdot \left(t_{wo}^{\ 2} + t_{air}^{\ 2}\right) \cdot \left(t_{wo} + t_{air}\right) \tag{16}$$

where: ε – housing emissivity coefficient which depends on the material, temperature and surface quality; σ - Stefan-Boltzmann constant $\left(\sigma = 5.67 \cdot 10^{-8}\, W/m^2K^4\right)$ [18].

If the lubricant velocity inside the housing $\left(\mathrm{w}_{lub}\right)$ is known, the coefficient of heat transfer (α_{lub}) from the lubricant to the inner wall of the housing (for the Reynolds number in the range of $5 \cdot 10^5 < R_{e,fi} < 10^7$) can be determined based on the expression [22]:

$$\alpha_{lub} = 0.037 \cdot R_{e,fi}^{\ 0,8} \cdot P_{r,fi}^{\ 1/3} \cdot \frac{\lambda_{lub}}{H_{wi}} \tag{17}$$

4.2 The amount of heat dissipated through the cylindrical wall of the housing

For one-dimensional heat flow through the cylindrical wall $\left(Q_{hc}\right)$, which receives heat from the lubricant by convection on the inside and transfers heat to the ambient air by convection and radiation on the outside (Figure 3), the following equations can be written [17-18]:

$$\mathrm{Q_{hc}} = \mathrm{R_{wi}} \cdot \pi \cdot \mathrm{L_c} \cdot \alpha_{lub} \cdot \left(t_{lub} - \mathrm{t_{wi,c}}\right) = 2\pi \cdot \mathrm{L_c} \cdot \frac{\lambda_w}{\ln\left(\frac{\mathrm{R_{wo}}}{\mathrm{R_{wi}}}\right)} \cdot \left(\mathrm{t_{wi,c}} - \mathrm{t_{wo,c}}\right) = \mathrm{R_{wo}} \cdot \pi \cdot \mathrm{L_c} \cdot \left(\alpha_{air,ccon} + \alpha_{air,rad}\right) \cdot \left(\mathrm{t_{wo,c}} - \mathrm{t_{air}}\right). \tag{18}$$

$$Q_{hc} = \frac{\left(t_{lub} - t_{wi,c}\right)}{1/\left(R_{wi} \cdot \pi \cdot L_c \cdot \alpha_{lub}\right)} = \frac{\left(t_{wi,c} - t_{wo,c}\right)}{ln\left(R_{wo} / R_{wi}\right) / 2\pi \cdot L_c \cdot \lambda_w} = \frac{\left(t_{wo,c} - t_{air}\right)}{1/\left(R_{wo} \cdot \pi \cdot L_c \cdot \left(\alpha_{air,ccon} + \alpha_{air,rad}\right)\right)} \tag{19}$$

$$Q_{hc} = \frac{\left(t_{lub} - t_{wi,c}\right)}{R_{c,lub}} = \frac{\left(t_{wi,c} - t_{wo,c}\right)}{R_{c,wal}} = \frac{\left(t_{wo,c} - t_{air}\right)}{R_{c,air}} \tag{20}$$

$$Q_{hc} = \frac{\left(t_{lub} - t_{air}\right)}{R_{c,total}} \tag{21}$$

$$R_{c,total} = R_{c,lub} + R_{c,wal} + R_{c,air} \tag{22}$$

where: $t_{wi,c}$ – temperature of the inner cylindrical wall of the housing; $t_{wo,c}$ – temperature of the outer cylindrical wall of the housing; R_{wi} – equivalent inner radius of the cylindrical housing wall $\left(R_{wi,ekv} = \left(\sum R_{wi} \cdot l_i\right) / \sum l_i\right)$; R_{wo} – equivalent outer radius of the cylindrical housing wall $\left(R_{wo,ekv} = \left(\sum R_{wo} \cdot l_i\right) / \sum l_i\right)$; L_c – length of the cylindrical housing; $\alpha_{air,ccon}$ – coefficient of convective heat transfer from the outer cylindrical housing wall to the ambient air; $R_{c,lub}$ – thermal resistance to heat transfer from the lubricant to the inner cylindrical wall; $R_{c,wal}$ – thermal resistance to heat transfer through the cylindrical wall; $R_{c,air}$ – thermal resistance to heat transfer from the outer cylindrical wall to the ambient air.

To determine the external coefficient ($\alpha_{air,ccon}$), Hilpert [25-26] suggested the following expression:

$$\alpha_{air,ccon} = \frac{N_{u,co} \cdot \lambda_{air}}{2R_{wo}} \tag{23}$$

$$N_{u,co} = C_2 \cdot R_{e,co}{}^{m} \cdot P_{r,co}{}^{\frac{1}{3}} \tag{24}$$

$$R_{e,co} = \frac{2R_{wo} \cdot W_{air} \cdot \rho_{air}}{\mu_{air}} \tag{25}$$

$$P_{r,co} = \frac{c_{p,air} \cdot \mu_{air}}{\lambda_{air}} \tag{26}$$

where: C_2 , m – constants dependent on the range of the Reynolds number, as stated in Table 2.

Table 2: Values of constants depending on the range of the Reynolds number [25]

$R_{e,co}$	C_2	m	$R_{e,co}$	C_2	m
$4 \cdot 10^{-1} \div 4 \cdot 10^{0}$	0.989	0.330	$4 \cdot 10^{3} \div 4 \cdot 10^{4}$	0.193	0.618
$4 \cdot 10^{0} \div 4 \cdot 10^{1}$	0.911	0.385	$4 \cdot 10^{4} \div 4 \cdot 10^{5}$	0.027	0.805
$4 \cdot 10^{1} \div 4 \cdot 10^{3}$	0.683	0.466			

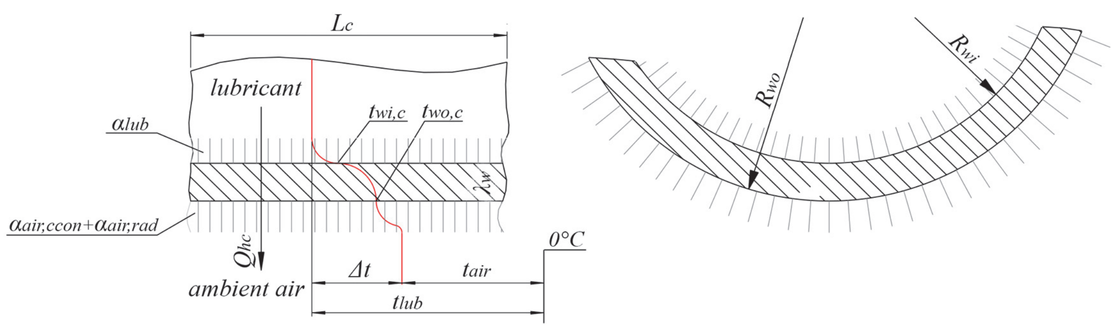

Figure 3: Heat dissipation through the cylindrical wall of the housing (Δt – the temperature difference between the lubricant and the ambient air)

5. MATHEMATICAL MODEL

After certain period of operation at constant torque, thermal equilibrium will be reached, i.e. the amount of mechanical energy converted into heat (Q_G) will equal the amount of heat dissipated (Q_R). This can be mathematically written as:

$$Q_G = Q_R \tag{27}$$

The amount of mechanical energy converted into heat can be determined based on the expression:

$$Q_G = P_{in} \cdot (1-\eta_{cr}) \tag{28}$$

where: P_{in} – input power, η_{cr} – efficiency of the cycloidal reducer.

However, for a simplified model where only heat transfer through the housing is taken into account, the amount of heat dissipated can be determined based on the expression:

$$Q_R = Q_{hf} + Q_{hc} \tag{29}$$

By equating the equations (28) and (29), a thermal equilibrium equation is obtained:

$$P_{in} \cdot (1-\eta_{cr}) = Q_{hf} + Q_{hc} \tag{30}$$

and by substituting the equations (6) and (21) in (30), a comprehensive expression is obtained in the following form:

$$P_{in} \cdot (1-\eta_{cr}) = \frac{(t_{lub} - t_{air})}{R_{f,lub} + R_{f,wal} + R_{f,air}} + \frac{(t_{lub} - t_{air})}{R_{c,lub} + R_{c,wal} + R_{c,air}} \tag{31}$$

After rearranging, the final expression for calculation of the lubricant equilibrium temperature is obtained, provided that all the heat is transferred through cylindrical and flat walls:

$$t_{lub} = \frac{P_{in} \cdot (1-\eta_{cr})}{\dfrac{1}{R_{f,lub} + R_{f,wal} + R_{f,air}} + \dfrac{1}{R_{c,lub} + R_{c,wal} + R_{c,air}}} + t_{air} \tag{32}$$

Under normal operating conditions, according to Castrol as one of the leading lubricant manufacturers, Optigear EP mineral oil provides good lubrication up to 88 ℃, Optigear Synthetic X PAO based synthetic oil ensures good lubrication up to 100 ℃, Optigear Synthetic 800 synthetic PAG based oil offers good lubrication up to 120 ℃, while Castrol Tribol GR 100-0 PD lithium grease based on mineral oil enables good lubrication up 140 ℃ [27-28]. However, in order to maintain the proper functioning of the cycloidal reducer (lubricants, seals, dilatation of components), the limit temperature should not exceed 65-70 ℃, i.e. it should not exceed the ambient temperature by more than 40℃ [29]. If the temperature is higher, it is necessary to install forced ventilation or increase the heat dissipation area.

6. MODEL TESTING AND SIMULATION RESULTS

This study was performed on a cycloidal reducer with the characteristics given in Table 3 [30]. In order to calculate the heat transfer coefficient $(\alpha_{air,rad})$, the value of the temperature was assumed $(t_{wo} = 80℃)$, while the other quantities were calculated using the given expressions.

Table 3: Basic characteristics of the cycloidal reducer

Characteristics	Value	Characteristics	Value
Input power, $P_{im}\ (kW)$	4	Coefficient of rolling friction, μ_{r1}	0.005
Input speed, $n_{im}\ (min^{-1})$	1420	Coefficient of rolling friction, $\mu_{r2} = \mu_{r3}$	0.0045
Reducer ratio, u_{CR}	13	Coefficient of sliding friction, $\mu_{s1} = \mu_{s2}$	0.05
Output torque, $T_{ou}\ (Nm)$	332	Coefficient of sliding friction, μ_{s3}	0.04

Pitch circle radius of the housing roller, $r\,(mm)$	86	Average air temperature, t_{air} $(℃)$	20
Eccentricity, $e\,(mm)$	4	Average air velocity, w_{air} (m/s)	1.25
Housing roller diameter, $D_0\,(mm)$	14	Thermal conductivity of the housing, λ_w (W/mK)	50
Diameter of the housing roller pin, $d_0\,(mm)$	8	Heat transfer coefficient for lubricant, α_{lub} $W/(m^2K)$	200
Number of output rollers, u	8	Outer surface area of the flat walls of the housing, $A_{wo,f}$ (m^2)	0.0832
Output roller diameter, $D_{VK}\,(mm)$	14	Outer surface area of the cylindrical walls of the housing, $A_{wo,c}$ (m^2)	0.1048
Diameter of the output roller pin, $d_{VK}\,(mm)$	7	Inner surface area of the flat walls of the housing, $A_{wi,f}$ (m^2)	0.0741
Diameter of the cycloid disc hole, $D_{OCZ}\,(mm)$	22	Inner surface area of the cylindrical walls of the housing, $A_{wi,c}$ (m^2)	0.0943
Pitch circle diameter of output rollers, R_{Oiz} (mm)	47.5	Equivalent thickness of the flat walls of the housing, δ_w (mm)	11
Inner diameter of the bearing, $d_{CZ}\,(mm)$	35	Equivalent radius of the outer cylindrical walls, R_{wo} (mm)	181
Outer diameter of the bearing, $D_{CZ}\,(mm)$	40	Equivalent radius of the inner cylindrical walls, R_{wi} (mm)	170
Emissivity coefficient of the housing, ε	0.8	Length of the cylindrical housing, $L_c\,(mm)$	150

Figure 4 shows the change in the lubricant equilibrium temperature (t_{lub}) in relation to the change in the load of the machine (T_{load}) working at a constant speed $(n_{ou} = 109.23\ min^{-1})$. The simulation was performed for three different heat transfer coefficients (α_{lub}) which varied in the range from 150 to 250 $W/(m^2K)$ and which depend on the following lubricant parameters: density (ρ_{lub}), flow velocity (w_{lub}), dynamic viscosity (μ_{lub}), kinematic viscosity (ν_{lub}), specific heat capacity at constant pressure $(c_{p,lub})$ and thermal conductivity coefficient (λ_{lub}). The load (T_{load}) varied in the range from 25 Nm to the nominal 332 Nm, while the overload of the electric motor was not simulated. A significantly higher lubricant temperature (t_{lub}) was obtained because the model lacked heat transfer through the foot, shafts and couplings. The temperature (t_{lub}) changes depending on the ratio between the amount of heat generated and the amount of heat dissipated. The values of the characteristic points in Figure 4 are shown in Table 4. With an increase in the load of the working machine (T_{load}), the impact of the value of the heat transfer coefficient (α_{lub}) on the lubricant equilibrium temperature (t_{lub}) increases.

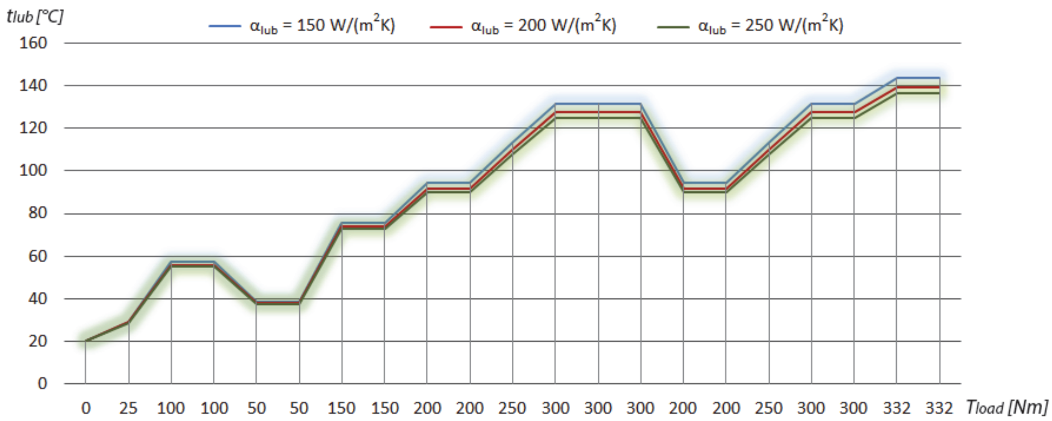

Figure 4: Lubricant equilibrium temperatures in relation to the ratio between the amount of heat generated and the amount of heat dissipated for different values of the heat transfer coefficient (α_{lub})

Table 4: Lubricant equilibrium temperatures at characteristic points for different values of the coefficient (α_{lub})

$T_{load}\,(Nm)$	0	25	50	100	150	200	250	300	332
$\alpha_{lub}=150\left(W/(m^2K)\right)$	22 ℃	29.3 ℃	38.59 ℃	57.22 ℃	75.81 ℃	94.44 ℃	113 ℃	131.6 ℃	143.5 ℃
$\alpha_{lub}=200\left(W/(m^2K)\right)$	22 ℃	28.96 ℃	37.92 ℃	55.87 ℃	73.79 ℃	91.74 ℃	109.7 ℃	127.6 ℃	139.1 ℃
$\alpha_{lub}=250\left(W/(m^2K)\right)$	22 ℃	28.76 ℃	37.52 ℃	55.06 ℃	72.57 ℃	90.12 ℃	107.6 ℃	125.1 ℃	136.4 ℃

Figure 5.a shows how the temperature difference between the lubricant and the outer wall of the housing ($t_{lub}-t_{wo}$) changes as a result of a change in the wall thickness (δ_w). For this simulation, the approximation $(R_{wi}=R_{wo}-\delta_w)$ was introduced. The load (T_{load}) had a constant value of 50 Nm, while the wall thickness varied in the range from 8 to 15 mm. Based on this simulation it can be concluded that the change in the wall thickness (δ_w) has no significant effect on the temperature difference. With an increase of 7 mm in the wall thickness (δ_w), the temperature difference increases by 0.108 ℃.

Figure 5.b shows the change in the lubricant equilibrium temperature (t_{lub}) in relation to the change of the coefficient of thermal conductivity (λ_w), which depends on the type of the housing material. The use of grey cast iron EN-GJL-200 ($\lambda_w = 48W/mK$) [31], cast steel GS-60 $(\lambda_w = 50W/mK)$ and aluminum alloy AlSi11Cu3 / ADC-12 $(\lambda_w = 92W/mK)$ [32] was analyzed. The load (T_{load}) varied in the range from 295 Nm do 296 Nm.

Based on this simulation, it can be concluded that aluminium alloy provides the best heat dissipation, while there is no significant difference between the grey cast iron and cast steel due to the extremely small surface area of the housing.

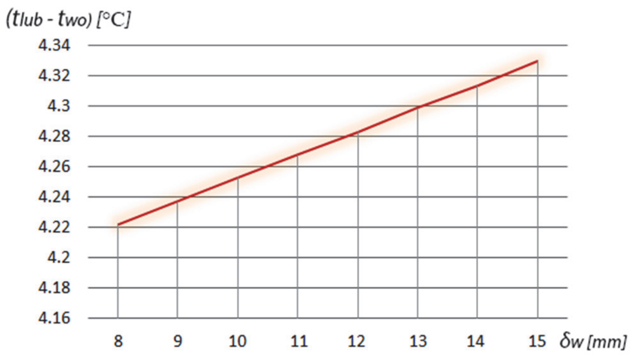

a)

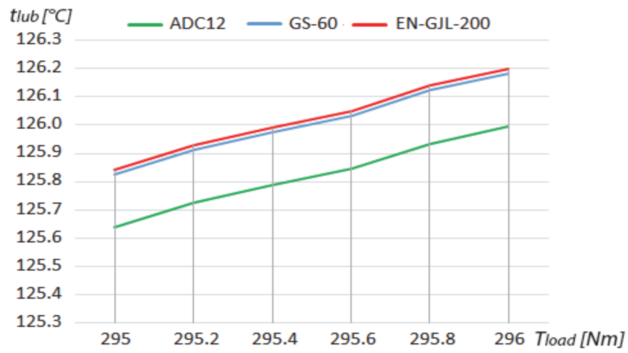

b)

Figure 5: (a) Dependence of the temperature difference $(t_{lub}-t_{wo})$ on the change in the housing wall thickness; (b) Dependence of the lubricant equilibrium temperature (t_{lub}) on the housing material

Figure 6. shows the change in the lubricant equilibrium temperature (t_{lub}) in relation to the change in the ambient air velocity (w_{air}). In case the gearbox is located indoors, the speed of 1.25 m/s is usually taken [33]. The operation of the gearbox located outdoors, where the values of the air velocity are 2 m/s and 3 m/s, was also analysed. The load (T_{load}) varied in the range from 300 Nm to the nominal 333 Nm. Based on this simulation, it can be concluded that the air velocity significantly affects the heat dissipation and the equilibrium temperature.

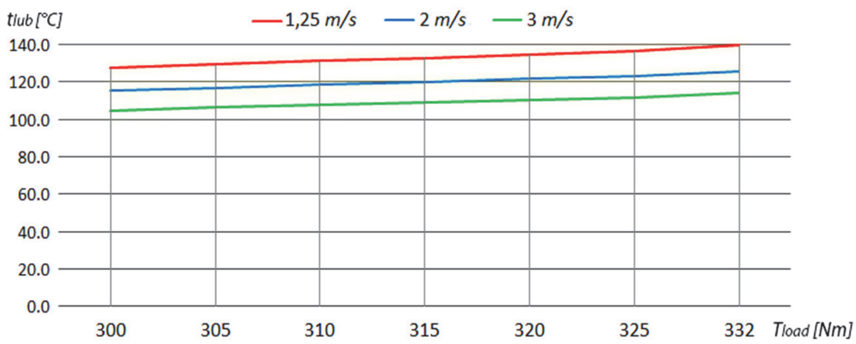

Figure 6: Dependence of the lubricant equilibrium temperature on the ambient air velocity

7. CONCLUSION

A model to predict both the amount of heat dissipated from the outer surface of the housing and the lubricant equilibrium temperature has been developed in this paper. The model is based on the correlation between the mechanical energy converted into heat and the amount of heat dissipated to the ambient air. Due to the specific geometry of the housing, two approximations have been introduced: that the housing is a homogeneous and isotropic medium with flat and cylindrical surfaces, and that the inner side of the housing is in contact only with a constant-temperature lubricant.

An actual cycloidal reducer with a nominal power of 4 kW, a nominal torque on the output shaft of 332 Nm and a transmission ratio of 13 was studied. Based on the testing performed, valuable conclusions have been drawn.

When the cycloidal reducer is loaded up to the nominal 332 Nm, the equilibrium temperature (t_{lub}) changes depending on the balance between the amount of heat generated and the heat dissipated. The value of the heat transfer coefficient (α_{lub}) has no significant effect at lower loads, but at higher loads its impact is prominent.

From the aspect of geometry, it can be noticed that the change in the wall thickness (δ_w) does not have significant effects on the temperature difference between the lubricant and the outer wall $(t_{lub} - t_{wo})$. With an increase in the wall thickness (δ_w) by 7 mm, the temperature difference increases by 0.108 ℃.

Tests on different housing materials have shown that aluminium alloy (AlSi11Cu3/ADC-12) provides the fastest heat dissipation, while with grey cast iron (EN-GJL-200) and cast steel (GS-60) the heat dissipation is much slower.

As for the weather conditions, the velocity of the air (w_{air}) significantly affects the heat dissipation and, consequently, the value of the equilibrium temperature (t_{lub}). By changing the velocity from 1.25 m/s to 3 m/s, at the same load, the equilibrium lubricant temperature (t_{lub}) decreases by 25 ℃.

Our further studies will be devoted to expanding the model to include the impact of the housing foot, shafts and couplings on the heat dissipation, as well as to performing experimental verification of the developed model.

ACKNOWLEDGEMENTS

This paper is a result of TR33015 project of the Ministry of Education, Science and Technological Development, in Serbia. The projects is titled "Research and Development of a Serbian Zero-Net Energy House". We would like to thank the Ministry of Education, Science and Technological Development on its financial support during this research.

REFERENCES

[1] M. Zah, D. Lates, V. Csibi, “Thermal Calculation for Planetary Cycloidal Gears with Bolts”, Elec. and Mech. Eng., Vol. 4, pp. 103-110, (2013)

[2] V. N. Kudryavcev, “Planetarnye peredachi” (in Russian), Masinostroenie, Moskva (Russia), (1966)

[3] S. K. Malhotra , M. A. Parameswaran, “Analysis of a cycloid speed reducer”, Mech. and Mach. Theo., Vol. 18 (6), pp. 491-499, https://doi.org/10.1016/0094-114X(83)90066-6, (1983)

[4] S. Bednarczyk, “Determining Power Losses in the Cycloidal Gear Transmission Featuring Manufacturing Deviations”, Proceedings of the 14th International Scientific Conference “Computer Aided Engineering”, Wroclaw (Poland), June, pp. 55-63, https://doi.org/10.1007/978-3-030-04975-1_7, (2018)

[5] F. Concli , L. Maccioni , C. Gorla, “Power loss analysis of different high-power density gearbox typologies: CFD analysis and experimental measurements on a cycloidal gear set”, 8th International Conference on Gear Production, Munich (Germany), 18th to 20th September, pp. 101-114, https://hdl.handle.net/10863/14094, (2019)

[6] M. Vasić, M. Matejić, M. Blagojević, “A comparative calculation of cycloid drive efficiency”, 5th international scientific conference "Conference on Mechanical Engineering Technologies and Application - COMETa", East Sarajevo (SR BiH), 26-28 November 2020, pp. 259-266, (2020)

[7] A. Mihailidis, E. Athanasopoulos, E. Okkas, “Flash temperature in cycloid reducers”, Jou. of the Bal. Trib. Assoc., Vol. 21 (1), pp. 76-89, (2015)

[8] A. Mihailidis, K. Agouridas, K. Panagiotidis, “Non-Newtonian Starved Thermal-Elastohydrodynamic Lubrication of Finite Line Contacts”, Trib. Tran., Vol. 56, pp. 88-100, http://dx.doi.org/10.1080/10402004.2012.729298, (2013)

[9] W. Li , Y. Hu, "Thermal analysis of cycloidal gear for the RV reducer", Jou. of Har. Eng. Univ., Vol. 38 (10), pp. 1560-1567, http://dx.doi.org/10.11990/jheu.201605085, (2017)

[10] K. Olejarczyk, M. Wiklo, K. Król, K. Kolodziejczyk, R. Nowak, "Experimental impact studies of the application mineral oil and synthetic oil on the efficiency of the single-gear cycloidal", Tribologia, Vol. 1 (1), pp. 067-073, http://dx.doi.org/10.5604/01.3001.0010.6365, (2017)

[11] C. Paschold, M. Sedlmair, T. Lohner, K. Stahl, "Efficiency and heat balance calculation of worm gears", Forsc. im Ingen., Vol. 84 (3), pp. 115–125, https://doi.org/10.1007/s10010-019-00390-1, (2020)

[12] J. Hermes, "Tragfähigkeit von Schneckengetrieben bei Anfahrvorgängen sowie Last- und Drehzahlkollektiven", PhD Thesis, Universität Bochum (GER), (2006)

[13] Đ. Miltenović, "Research of thermal stability and wear of worm gear" (in Serbian), PhD Thesis, University of Banja Luka (SR BiH), (2017)

[14] H. Xue, H. Xu, "Simulation calculation of temperature field of gearbox in straddle monorail train", Jou. of Phy.: Con. Ser., Vol. 2174, pp. 1-8, https://iopscience.iop.org/article/10.1088/1742-6596/2174/1/012074, (2022)

[15] P. Živković, M. Ognjanović, "Thermal balance of planetary gear drives" (in Serbian), Res. and Dev. of Mec. Ele. and Sys. "IRMES '06", Banja Luka (SR BiH), 21-22. September, pp. 199-204, (2006)

[16] A. Mihailidis, E. Athanasopoulos, K. Agouridas, "EHL film thickness and load dependent power loss of cycloid reducers", Jou. Mech. Engin. Scie., Vol. 230 (7–8), pp. 1303–1317, https://doi.org/10.1177/0954406215612815, (2016)

[17] M. Bojić, E. Hnatko, "Thermotechnics" (in Serbian), Faculty of Engineering of Kragujevac, Bor (Serbia), (1987)

[18] R. J. Crawford, J. L. Throne, "Rotational Molding Technology", William Andrew, Norwich (New York), (2001)

[19] D. Jelaska, "Gears and Gear Drives", John Wiley & Sons Ltd, Split (Croatia), https://doi.org/10.1002/9781118392393, (2012)

[20] ISO/TR 14179-2, Gears — Thermal capacity — Part 2: Thermal load-carrying capacity, (2001)

[21] DIN 1681 Grade GS-60 heat treated. URL: https://matmatch.com/materials/minfm31143-din-1681-grade-gs-60-heat-treated (Accessed on: 2022-05-18)

[22] C. H. Forsberg, "Heat Transfer Principles and Applications", Academic Press, London (United Kingdom), (2021)

[23] S. W. Churchill, H. H. S. Chu, "Correlating equations for laminar and turbulent free convection from a vertical plate", Inr. J. He. Mo. Tra., Vol. 18 (11), pp. 1323-1329, https://doi.org/10.1016/0017-9310(75)90243-4, (1975)

[24] P. Živković, "Energy losses and failure of planetary gears' parts research" (in Serbian), PhD Thesis, Faculty of Mechanical Engineering of the University of Belgrade (Serbia), (2006)

[25] Y. Bai, Q. Bai, "Subsea Engineering Handbook", Gulf Professional, Burlington (USA), (2010)

[26] R. Hilpert, "Wärmeabgabe von geheizten Drähten und Rohren im Luftstrom", Fors. auf dem Geb. des Inge. A, Vol. 4, pp. 215–224, https://doi.org/10.1007/BF02719754, (1933)

[27] Gear oils. URL: https://testing.volume.co.uk/50636/page-templates/product-families/gear-oils.html (Accessed on: 2022-05-21)

[28] Reduction Gear Grease Vigogrease RE0. URL: www.motionsolutions.com/store/pc/catalog/documents/grease/VigoTechDataAnalysis.pdf (Accessed on: 2022-05-21)

[29] TwinSpin and DriveSpin catalogue, Edition II/2019. URL: https://www.graessner.at/upload/41432244-Catalogue-TwinSpin-and-DriveSpin.pdf (Accessed on: 2022-05-15)

[30] M. Blagojević, "Kinematic and dynamic analysis of single - stage cyclo speed reducer" (in Serbian), Master's thesis, Faculty of Engineering University of Kragujevac (Serbia), (2003)

[31] Grey cast iron. URL: https://www.vonroll-casting.ch/en/grey-cast-iron.html (Accessed on: 2022-05-18)

[32] ADC12 Aluminum A383 | Equivalent Materials & Metal Specifications. URL: https://redstonemanufacturing.com/adc12-aluminum/ (Accessed on: 2022-05-18)

[33] V. Miltenović, M. Ognjanović, "Machine elements II: power transmission elements" (in Serbian), Faculty of Mechanical Engineering – University of Niš, Niš (Serbia), (1995)

ORIGINAL SCIENTIFIC PAPER OPEN ACCESS

Possibilities for reduction of energy consumption by replacing public lighting with LED lighting: case study of Priboj municipality

Ana Radojević[1], Marko Janjušević[2], Danijela Nikolić[1*], Gordana Bogdanović[1], Lozica Ivanović[1], Jasmina Skerlić[3], Zuzana Palkova[4]

[1] University of Kragujevac, Faculty of Engineeing, Kragujevac, Serbia

[2] Priboj City Government, Priboj, Serbia

[3] University of Priština temporarily settled in Kosovska Mitrovica, Faculty of Technical Sciences, Kosovska Mitrovica, Serbia

[4] Slovak University of Agriculture in Nitra, Technical Faculty, Nitra, Slovakia

ARTICLE INFO

[*] **Correspondence:** danijela1.nikolic@gmail.com

DOI: 10.5937/engtoday2202019R

UDC: 621(497.11) **ISSN:** 2812-9474

Article history: Received 02 June 2022; Accepted 19 June 2022

ABSTRACT

Electric energy consumed by the public lighting represents a significant item in the city public sector energy consumption structure, which includes public buildings, public transportation and public lighting. Public lighting system is one of the most important public utility activities which is under control of local governments, which pay the costs of electricity, as well as maintenance costs. Public lighting affects the quality of life of citizens in cities through, among other things, reduction of traffic accidents by up to 35%, personal safety and reduction of social approaches.

Cities and municipalities in Serbia are predominately using sodium and mercury bulbs for public lighting, but have been gradually replacing them with LED bulbs in the recent years. LED technology is a satisfactory, cost-effective solution due to low energy consumption, long service life, reduced investment and maintenance costs. Thus, there is not only a reduction in energy consumption of up to 70%, but also a large reduction in CO_2 emissions. The modernization of the public lighting system is, in addition to being a useful means of achieving significant energy savings, also a means of improving the quality of lighting itself.

The paper shows how much it is possible to reduce electricity consumption, and thus CO_2 emissions, by replacing existing lighting with LED lighting. There are 2530 light bulbs in the public lighting system of the municipality of Priboj. Until recently, mercury high pressure bulbs dominated – there were 1241 of them, compared to 743 sodium ones and 546 LED lamps. After the reconstruction of public lighting, all light bulbs are LED. The paper compares the consumption of electricity for the four months of 2019 and the same four months of 2020. It is shown that electricity consumption for these four months was reduced by an average of 55%, the average reduction in CO_2 emissions was 55%, while the reduction in electricity costs was an average of 58%.

KEYWORDS

Public lighting, Energy consumption, Energy saving, Reduction of CO_2 emissions.

1. INTRODUCTION

The possibilities for saving energy in street lighting are very significant, because changes can reduce electricity consumption by more than 50% [1]. By replacing street lighting, in addition to saving energy, visual comfort and safety are improved [2]. One of the most common measures is the replacement of light sources with more efficient LED lamps, which is increasingly becoming a satisfactory and cost-effective solution due to its low energy consumption [3], long life, reduced investment costs [4] and maintenance costs [5], less environmental impact [6] and many other advantages.

In terms of uniformity of street lighting and the comfort it provides, the results show the positive effects of LED street lighting on the surveyed pedestrians and vehicle drivers, as shown by a study conducted for the city of Vienna [7]. When comparing LED lighting and HPS lamps, the results of the analysis for the possibility of improving road lighting standards in Thailand [8], show that the LED lamp has a better energy saving effect than HPS lamp (reduction of energy efficiency index by approximately 40% compared to HPS lamp), which indicates that municipalities and cities benefit from the use of LED lamps. However, although the lighting quality results for LED lamps have values approximately the same as those of the standard ones, the lighting quality needs to be improved in terms of uniformity. In an another research, within the analysis of the optimal lighting solutions characterized by the lowest installed power, it was shown that when considering mesopic effects the average energy savings achieved comparing LED (NW and WW) with HPS lighting solutions amounted to 41–62% and 29–59%, respectively, while the ratio between the total costs of the comparable LED (NW and WW) and HPS lighting solutions belonged to the ranges 0.59–1.26 and 0.61–1.14, respectively. [9] It has also been observed that improvement in areas with poor lighting systems can reduce traffic accidents by up to 35% [10].

The public lighting system is an important municipal function not only because of energy consumption/savings and traffic safety, but also because of its great role in public health and social welfare [11]. Moreover, it is significantly effective in reducing crime and strengthening personal security [12], as well as in overall social well-being [13].

Public lighting also plays a significant role in creating smart cities. The research [14] shows that unlike conventional lighting control systems, that focus only on controlling the lighting levels, the introduced method provides a more effective control solution. The accuracy of this technique is supported by the results of system simulation and implementation. The proposed method is recommended as a novel strategy for meeting the requirements of smart grids, smart cities, and unregulated energy markets.

Also, there is a connection between using two types of warm white and cool white in smart cities [15]. The proposed method benefits from two types of warm white and cool white LEDs and their input power control to adjust the luminous flux and resulting correlated color temperature of light-emitting diodes. The simulation findings confirm the performance of the introduced method. This technique is recommended as a novel strategy, especially to meet the requirements of inhabitants of smart cities.

Public lighting connects hundreds of millions of streetlights with access to power across the globe, being responsible for 19% of global electricity usage, 30% - 50% of a typical city's energy bill and the already exceeding levels of CO_2 emissions [16]. Nowadays, 5.56% of the energy generated in Ecuador is destined to the public lighting service [17]. In Brazil, the public lighting sector is a responsibility of the municipal government and typically represents around 4% of the electricity consumed by cities [18].

In Serbia, as well as in the surrounding countries, costs for public lighting in municipal/city budgets are a significant item – the public lighting in the city of Rijeka, in Croatia, for example, takes about 3% of total electricity consumption in the city, which is a significant cost for municipal budgets [19].

Due to all the above, it is necessary to replace outdated street lighting with modern LED lighting. However, the improvement and modernization of public lighting systems in cities and municipalities is often hampered by high perceived investment risks, long payback periods and a lack of capacity for local governments to implement these projects themselves. At the municipal level, these issues are particularly pronounced because the procurement, implementation and management of retrofitting may exceed existing municipal management capacities. Therefore, public-private partnership is emerging as one of the solutions for improving the public lighting system and energy efficiency in cities and municipalities [20].

2. PRIBOJ MUNICIPALITY CASE STUDY

2.1. Electric Power Consumption in Public Sector

Electricity consumption in the public sector includes electricity consumption in public buildings and public lighting. The analysis of consumption in the period of four years (2016-2019) shows that the share of electricity consumption for public lighting was 60% higher than the share of electricity consumption in public buildings.

During the 2016 and 2017, electricity consumption in public buildings in Priboj municipality was 1,092,579 kWh and 1,136,660 kWh, respectively, while electricity consumption in public lighting was 1,644,541 kWh and 1,610,204 kWh, respectively. In 2018 and 2019, electricity consumption in the public sector in Priboj municipality was a little less. Public buildings electricity consumption in 2018 and 2019 was 1,099,518 kWh and 1,137,884 kWh, respectively (slightly increased, compared to the previous two years), while electricity consumption in public lighting was significantly reduced, i.e. 1,306,939 kWh and 1,306,048 kWh, respectively.

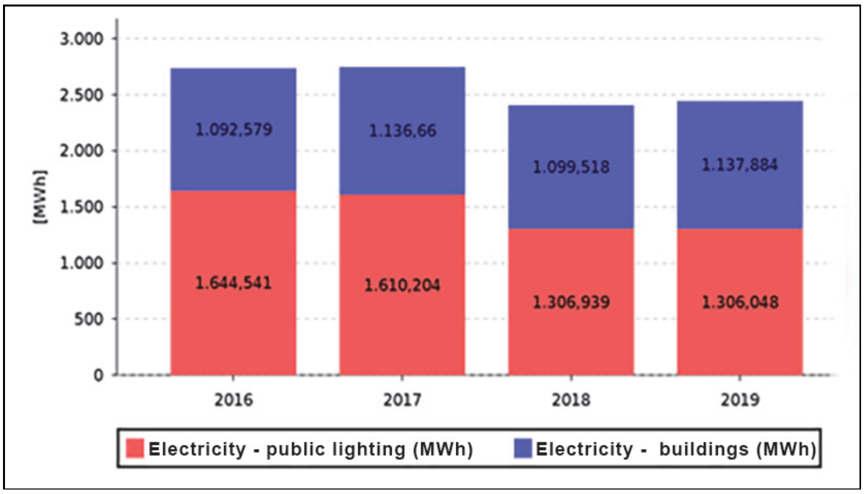

Figure 1: Structure of electricity consumption in the public sector before lamp replacement

2.2. Previous situation in public lighting

The main characteristics of the public lighting system in the municipality of Priboj were mostly inefficiency and obsolescence, and as such, the system did not provide quality lighting. There were high costs for energy and maintenance. In addition, the function of the system was significantly impaired by years of insufficient or poor maintenance.

The maintenance of the public lighting system carried out by the municipality included the replacement of light sources (bulbs) and other parts of lamps (ballasts, bulb sockets, glass protectors), replacement of damaged lamps, replacement of damaged poles and cable installations, replacement of damaged parts of control units (meters, contactors, photo relays, astronomical clocks, fuses) and, if necessary, system expansion.

Table 1: Condition of lamps before replacement

STRUCTURE OF LAMPS	NUMBER OF LAMPS	INSTALLED POWER (in kW)
Mercury 125M	998	137.23
Mercury 250M	243	66.83
Sodium 70M	595	45.82
Sodium 100M	36	3.96
Sodium 150M	33	5.45
Sodium 250M	48	13.20
Spotlight MX 30	1	0.03
Spotlight MX 150	10	1.65
Spotlight MX 250	4	1.10
Spotlight MX 400	2	0.88
Spotlight HA 250	4	1.10

Spotlight HA 400	10	4.40
Existing LED 28	64	1.79
Existing LED 39	57	2.22
Existing LED 57	152	8.66
Existing LED 84	202	16.97
Existing LED 110	20	2.20
Existing LED spotlight 50	7	0.35
Existing LED spotlight 100	16	1.60
Existing LED spotlight 400	28	11.20
TOTAL:	**2,530**	**326.62**

On the whole, the quality of maintenance of the public lighting system was insufficient, which resulted in insufficient quality of the lighting itself. This situation endangered the safety of all participants in traffic, and the problem of inadequate lighting particularly posed the problem for the traffic safety of children - pedestrians.

Table 1 shows the condition of the lamps before the replacement of the bulbs - the total number of lamps and the total installed power.

Figure 2 represents the percentage structure of public lighting in the municipality of Priboj. As it can be seen, the existing lighting was dominated by mercury bulbs with 49.05% and sodium bulbs with 28.14%.

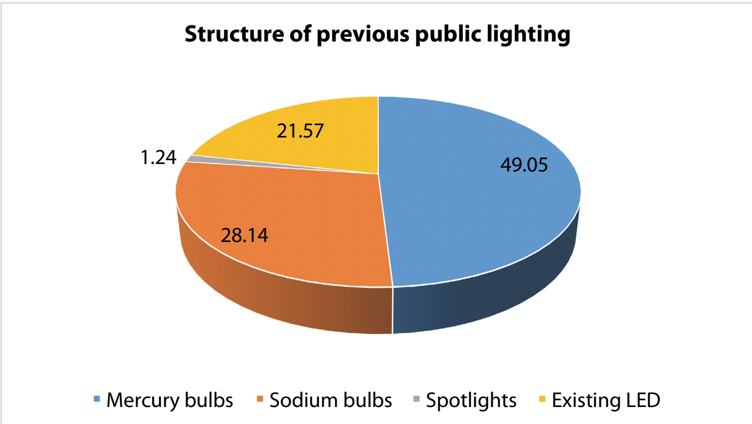

Figure 2: Structure of public lighting before light bulb replacement

2.3. Improved condition

When drafting the reconstruction proposal and finding the optimal lighting solution, the following principles were followed:

- to rely on the existing electrical installation for the solution,
- to propose a rational solution that meets the necessary lighting criteria relating to a given category of road, to the extent that the current network infrastructure allows it,
- to meet the required levels of illumination with adequate installed equipment, meaning that it is necessary to use the highest quality lamps and to meet the applicable standards and regulations regarding the illumination of roads.
- to significantly reduce electricity consumption.

In addition to the choice of lamps, it is important to consider the method of managing the public lighting system. The following results are achieved by managing public lighting:

- reduction of energy consumption and CO_2 emissions,
- reduction of light pollution,
- reduction of maintenance costs.

By installing an appropriate control system, it is possible to provide night control of lighting and reduce the intensity of light emitted by each lamp, while maintaining uniformity of illumination. There are different systems for managing public lighting. The most economical way to regulate night lighting is through built-in automatic dimmers in the lamps. It is a tested technology that has been functioning reliably for many years. The rate of failures in newly installed luminaires is minimal and they are eliminated by a private partner during the term of the contract.

The analysis of the data obtained by field measurements, which are shown in Table 1, established the exact number of lamps that are the subject of reconstruction and calculated the exact installed power. When choosing new lamps, it was made sure that they have good photometric characteristics, a high degree of mechanical and electrical protection, made of quality and unbreakable materials, which ensures a long service life.

During the public-private partnership, the private partner prepares project documentation, procurement, transport and installation of equipment, managing the replacement of existing lamps for energy efficient LED lamps, disposal of old equipment in a place determined by the public partner, financing, insurance (in the first year) and maintenance of the project and public lighting system for the duration of the contract, with the aim of reducing budget costs and raising the level of efficiency in the provision of public services. The project is fully financed from the potential of a private partner - there are no investments for local self-government.

The analysis of the categorization of roads and the number of existing luminaires determined the exact number of LED luminaires needed for the reconstruction of public lighting and their installed power. Based on these principles, Table 2 shows the newly designed solution.

Table 2: Condition of lamps after replacement

Type of lamp and its power (W)	Total Number	Total Installed Power in (kW)	Total dimmed installed power in (kW)
NEW LED 80 W	99	7.92	6.73
NEW LED 60 W	359	21.54	18.31
NEW LED 45 W	17	0.77	0.65
NEW LED 40 W	994	39.76	33.8
NEW LED 25 W	484	12.1	12.1
NEW REF 60 W	11	0.66	0.66
NEW REF 100 W	20	2.00	2.00
LED REF 50 W*	7	0.35	0.35
LED REF 100W*	16	1.6	1.6
LED REF 400W*	28	11.2	11.2
LED LAMP.28W*	64	1.79	1.79
LED LAMP 39W*	57	2.22	2.22
LED LAMP 57W*	152	8.66	8.66
LED LAMP 84W*	202	16.97	16.97
LED LAMP 110W*	20	2.2	2.2
TOTAL	**2530**	**129.74**	**119.24**

Estimated financial savings:

After the reconstruction, the Municipality of Priboj in the first year should achieve guaranteed savings of at least 1389293 RSD or 11675 EUR, which is 10% of current expenditures on the electricity bill annually. The estimated financial savings during the 15-year contract should reach about 26 million RSD for the Municipality of Priboj (in case there is no increase in electricity prices in the next 15 years, which is unlikely).

3. ACHIEVED SAVINGS

Table 3 shows electricity consumption and energy savings for public lighting in the municipality of Priboj, in 2019 and 2020.

Table 3: Savings in electricity consumption

Period	Electricity consumption for public lighting in 2019 (kWh)
September 2019	97,129
October 2019	136,984
November 2019	128,850
December 2019	148,365
TOTAL ELECTRICITY CONSUMPTION IN 4 MONTHS OF 2019 (kWh)	**511,328**

Period	Electricity consumption for public lighting in 2020 (kWh)
September 2020	44,017
October 2020	57,052
November 2020	60,392
December 2020	70,718
TOTAL ELECTRICITY CONSUMPTION IN 4 MONTHS OF 2020 (kWh)	**232,179**
Period	Electricity savings (kWh)
September 2020	53,112
October 2020	79,932
November 2020	68,458
December 2020	77,647
TOTAL ELECTRICITY SAVINGS (kWh)	**279,149**
Period	Electricity savings (%)
September 2020	55
October 2020	58
November 2020	53
December 2020	52
AVERAGE ELECTRICITY SAVINGS (%)	**55**

Savings in electricity consumption amount from 53 112 kWh to a maximum of 79 932 kWh, which is a percentage of 52-58%, an average of 55% for the four analyzed months. Figures 3 shows the graphical presentation of reduction of electricity consumption for public lighting, for the analyzed period (September 2019-December 2020).

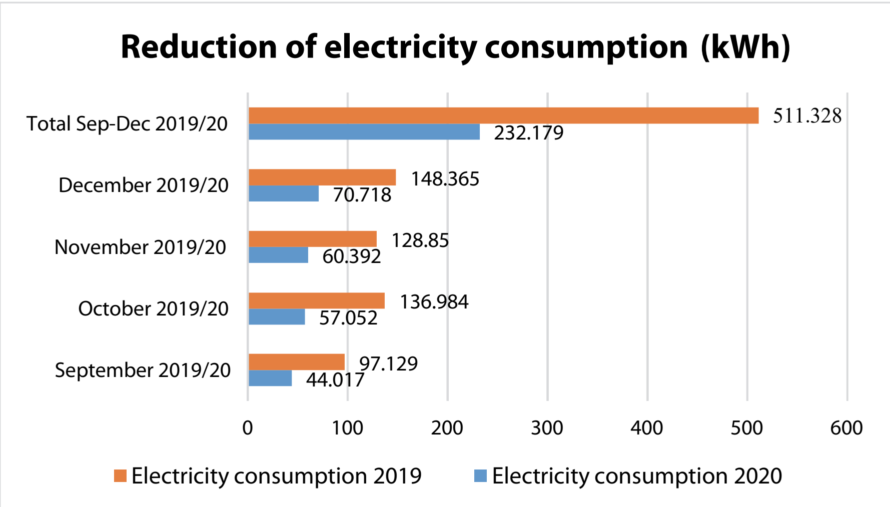

Figure 3: Reduction of electricity consumption – comparison between previous and new public lighting system

Table 4 shows reduction of CO_2 emission for public lighting in the municipality of Priboj, for the period from September 2019 to December 2020.

Table 4: CO_2 emission savings

Period	CO_2 emission in 2019 (tCO_2)
September 2019	106.84
October 2019	150.68
November 2019	141.74
December 2019	163.20
TOTAL CO_2 EMISSION IN 4 MONTHS OF 2019 (tCO_2)	**562.46**
Period	CO_2 emission in 2020 (tCO_2)
September 2020	48.42
October 2020	62.76
November 2020	66.43
December 2020	77.79

TOTAL CO_2 EMISSION IN 4 MONTHS OF 2020 (tCO_2)	**255.40**
Period	CO_2 emission reduction (tCO_2)
September 2020	58.42
October 2020	87.93
November 2020	75.30
December 2020	85.41
TOTAL CO_2 EMISSION REDUCTION (tCO_2)	**307.06**
Period	CO_2 emission reduction (%)
September 2020	55
October 2020	58
November 2020	53
December 2020	52
AVERAGE CO_2 EMISSION REDUCTION (%)	**55**

Results, obtained after installing the new LED lamps, in analyzed period, show the reduction in CO_2 emissions in range from 58.42 tCO_2 to 87.93 tCO_2. As a percentage, the reduction in CO_2 emissions is up to 52 to 58%, which is an average of 55%.

Figure 4 shows reduction of CO_2 emissions in a case of municipality of Priboj, after installing LED lamps, for the same period as electricity consumption (from September 2019 to December 2020). It can be concluded that a significant reduction in CO_2 emissions is achieved with new LED lamps, compared to the previous system of public lighting with dominant mercury bulbs and sodium bulbs.

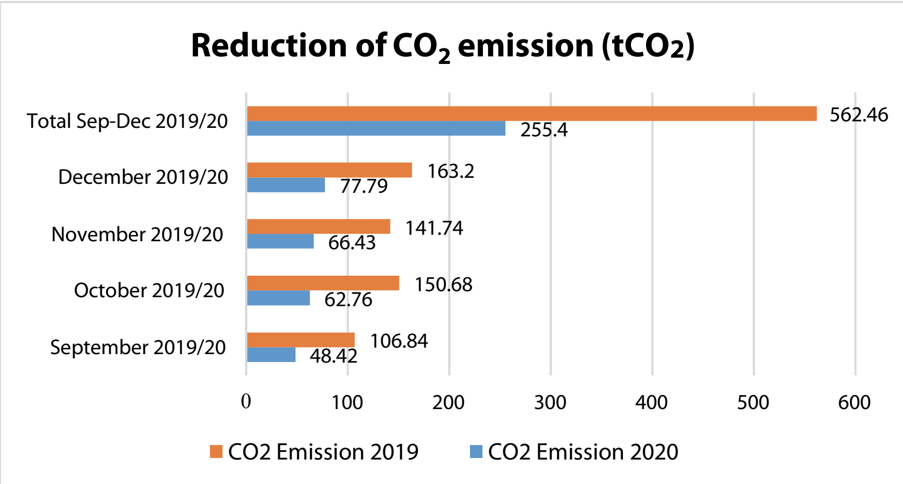

Figure 4: Reduction of CO_2 emissions - comparison between previous and new public lighting system

Table 5 shows electricity cost reductions, obtained with LED lamps in the municipality of Priboj, for the period from September 2019 to December 2020.

Table 5: Savings in electricity costs

Period	Cost of electricity for public lighting in 2019 (RSD)
September 2019	1,136,164.47
October 2019	1,604,476.30
November 2019	1,508,681.19
December 2019	1,737,011.62
TOTAL ELECTRICITY COSTS IN 4 MONTHS OF 2019:	**5,986,333.58**
Period	Cost of electricity for public lighting in 2020 (RSD)
September 2020	471,923.17
October 2020	611,085.91
November 2020	646,711.74
December 2020	757,052.07
TOTAL ELECTRICITY COSTS IN 4 MONTHS OF 2020:	**2,486,772.89**

Period	Savings in electricity costs for public lighting (RSD)
September 2020	664,241.30
October 2020	993,390.39
November 2020	861,969.45
December 2020	979,959.55
TOTAL SAVINGS IN ELECTRICITY COSTS:	**3,499,560.69**
Period	Savings in electricity costs for public lighting (%)
September 2020	58%
October 2020	62%
November 2020	57%
December 2020	56%
AVERAGE SAVINGS IN ELECTRICITY COSTS	**58%**

Savings in electricity costs on a monthly basis amount to 664,241.30 to 979,959.55 dinars. As a percentage, savings range from 56 to 62%, averaging 58% on a monthly basis compared to the same period previous year.

Figure 5 shows the structure of electricity consumption in the last five years and shows that the share of electricity consumption for public lighting was 60% higher than the share of electricity consumption in public buildings in 2016, and in 2020 consumption was higher for public buildings than for public lighting.

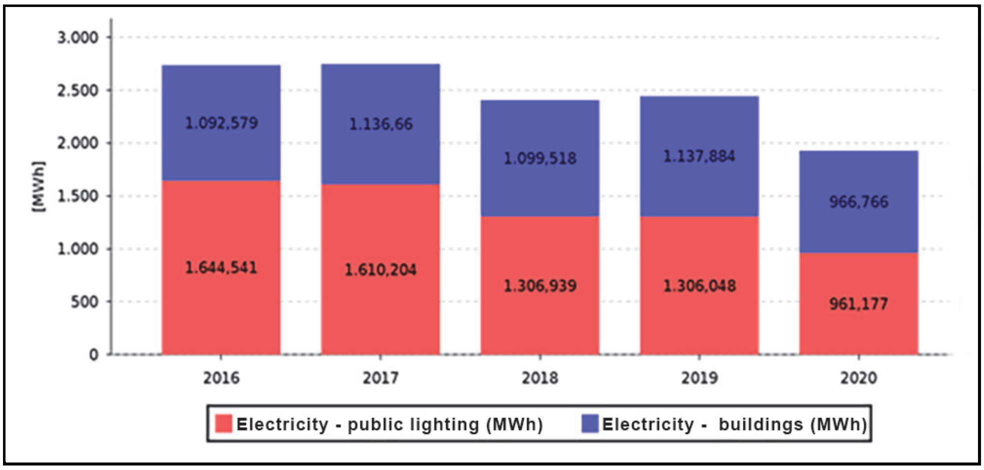

Figure 5: Structure of electricity consumption in the public sector before and after lamp replacement

4. CONCLUSION

The replacement of existing light sources with more efficient LED lamps is increasingly becoming a satisfactory and cost-effective solution due to its low energy consumption, long life, improved quality of lighting, and thus increased general safety and satisfaction of citizens, reduced investment and maintenance costs, lower environmental impact and many other benefits. Better quality of life of citizens is achieved through greater safety in traffic, both for pedestrians and drivers, and by reducing the number of traffic accidents. New LED lighting also affects general security, reduces social crime and strengthens personal security. In addition, new LED lighting contributes to the creation of smart cities. At the same time, as it is a public-private partnership project, quality maintenance by a private partner and quality management of the public lighting system is achieved.

This paper represents the possibility for reduction of electricity consumption and thus CO_2 emissions, by replacing existing lighting with LED lighting, in a case of public lighting system of the municipality of Priboj. The savings achieved are: reduction of electricity consumption in four months period by an average of 55%, average reduction of CO_2 emissions by 55%, while reduction of electricity costs is averagely 58%. These results clearly show the importance of replacing obsolete public lighting devices with new ones, both in terms of energy saving and emission reduction, as well as in financial term.

ACKNOWLEDGEMENTS

This research is part of the projects TR 33015, TR 35033 and III 42006. The authors would like to thank to the Ministry of Education, Science and Technological Development of Republic of Serbia for the financial support during this research.

REFERENCES

[1] J.A. Lobão, T. Devezas and J.P.S. Catalão, "Energy efficiency of lighting installations: software application and experimental validation", Energy Reports, pp. 110-115, https://doi.org/10.1016/j.egyr.2015.04.001, (2015)

[2] S. Ferrar and M. Beccali, "Energy-environmental and cost assessment of a set of strategies for retrofitting a public building toward nearly zero-energy building target", Sustainable Cities and Society, pp. 226-234, https://doi.org/10.1016/j.scs.2017.03.010, (2017)

[3] M.Beccali, M.Bonomolo, V.Lo Brano, G.Ciulla, V.Di Dio, F.Massaro and S.Favuzza, "Energy saving and user satisfaction for a new advanced public lighting system", Energy Conversion and Management, Vol.195, pp. 943-957, https://doi.org/10.1016/j.enconman.2019.05.070, (2019)

[4] S. Li, Y. Jiang and B. Guan, "Field evaluation of light performance for new light sources in roadway lighting applications", pp. 372-385, Journal of Traffic and Transportation Engineering, (2014)

[5] D. Campisi, S. Gitto and D. Morea, "Economic feasibility of energy efficiency improvements in street lighting systems in Rome", Journal of Cleaner Production, pp. 190-198, https://doi.org/10.1016/j.jclepro.2017.12.063, (2018)

[6] L. Tähkämö and L. Halonen, "Life cycle assessment of road lighting luminaires comparison of light-emitting diode and high-pressure sodium technologies", Journal of Cleaner Production, pp. 234-242, https://doi.org/10.1016/j.jclepro.2015.01.025, (2015)

[7] K. Markvica, G. Richter and G. Lenz, " Impact of urban street lighting on road users' perception of public space and mobility behavior", Building and Environment, Vol. 154, pp. 32-43, https://doi.org/10.1016/j.buildenv.2019.03.009, (2019)

[8] S. Yoomak, C. Jettanasen, A. Ngaopitakkul, S. Bunjongjit and M. L. Lajindakrairerk, "Comparative study of lighting quality and power quality for LED and HPS luminaires in a roadway lighting system", Energy and Buildings, Vol. 159, pp. 542-557, https://doi.org/10.1016/j.enbuild.2017.11.060, (2018)

[9] M. Davidovic, M. Kostic, "Comparison of energy efficiency and costs related to conventional and LED road lighting installations", Energy, Available online, p. 124299, https://doi.org/10.1016/j.energy.2022.124299, (2022)

[10] M. Jackett, W. Frith, **"**Quantifying the impact of road lighting on road safety - in A New Zealand Study"**,** IATSS Res., pp. 139-145, https://doi.org/10.1016/j.iatssr.2012.09.001, (2013)

[11] M. J. Mirzaei, R. Dashti, A. Kazemi and M. H. Amirioun, "An asset-management model for use in the evaluation and regulation of public-lighting systems", Utilities Policy, Vol. 32, pp. 19-28, https://doi.org/10.1016/j.jup.2014.12.001, (2015)

[12] O. Rabaza, *et al.*, "A simple method for designing efficient public lighting, based on new parameter relationships" Expert Systems with Applications, https://doi.org/10.1016/j.eswa.2013.07.037, Volume 40, 2013, pp. 7305-7315

[13] A. Haans and Y. AW. de Kort, "Light distribution in dynamic public lighting: two experimental studies on its effects on perceived safety, prospect, concealment, and escape", Journal of Environmental Psychology, pp. 342-352, https://doi.org/10.1016/j.jenvp.2012.05.006, (2012)

[14] J. Kalani and M. Kalani, "Energy cost control of LEDs considering the price of electricity and the desired lighting levels to meet the requirements of smart grids, smart cities, and unregulated energy markets", Optik, Vol. 258, p. 168926, https://doi.org/10.1016/j.ijleo.2022.168926, (2022)

[15] J. Kalani and M. Kalani, "Adaptive correlated color temperature control of LEDs considering ambient sound variations as a novel strategy to meet the requirements of inhabitants of smart cities", Optik, Vol. 261, p. 169193, https://doi.org/10.1016/j.ijleo.2022.169193, (2022)

[16] F. Pardo-Bosch, A. Blanco, E. Sesé, F. Ezcurra and P. Pujadas, "Sustainable strategy for the implementation of energy efficient smart public lighting in urban areas: case study in San Sebastian", Sustainable Cities and Society, Vol. 76, p. 103454, https://doi.org/10.1016/j.scs.2021.103454, (2022)

[17] S. G. Pulla, D. Borge-Diez and D. Icaza, "Energy sector in Ecuador for public lighting: Current status", Energy Policy, Vol. 160, p. 112684, https://doi.org/10.1016/j.enpol.2021.112684, (2022)

[18] A. L. Salvia, L. L. Brandli, W. L. Filho and R. M. L. Kalil, "An analysis of the applications of Analytic Hierarchy Process (AHP) for selection of energy efficiency practices in public lighting in a sample of Brazilian cities", Energy Policy, Vol. 132, pp. 854-864, https://doi.org/10.1016/j.enpol.2019.06.021, (2019)

[19] D. Radulovic, S. Skok and V. Kirincic, “Energy efficiency public lighting management in the cities”, Energy, Vol. 36, No. 4, pp. 1908-1915, https://doi.org/10.1016/j.energy.2010.10.016, (2011)

[20] F. P. P. von Flotow and C. Nolden, “Modes of governance for municipal energy efficiency services – The case of LED street lighting in Germany” in Journal of Cleaner Production Vol. 139, pp. 133-145, https://doi.org/10.1016/j.jclepro.2016.07.100, (2016)

ORIGINAL SCIENTIFIC PAPER OPEN ACCESS

Finite element modelling of laminated composite: effects of different ply orientations

Dragan Čukanović[1], Gordana Bogdanović[2*], Aleksandar Radaković[3]

[1] University of Priština in Kosovska Mitrovica, Faculty of Technical Sciences, Kosovska Mitrovica, Serbia

[2] University of Kragujevac, Faculty of Engineering, Kragujevac, Serbia

[3] State University of Novi Pazar, Novi Pazar, Serbia

ARTICLE INFO

[*] **Correspondence:** gocab@kg.ac.rs

DOI: 10.5937/engtoday2202029C

UDC: 621(497.11) **ISSN:** 2812-9474

Article history: Received 08 June 2022; Accepted 25 June 2022

ABSTRACT

The subject of analysis in this paper are laminated composites as an always popular topic in the field of composite materials. The introductory part of the paper presents a brief overview of the current state of research in this area and points out further directions of research related to this very interesting topic. The classification of laminated composite plates from the aspect of different criteria are described in detail. As the subject of the paper is stress-strain analysis of laminated composite, the expression for the generalized Hooke's law of orthotropic class of material symmetry is given. The terms of the constitutive matrix are expressed through engineering constants. At the end, the bending analysis of the rigidly supported laminated plate under a sinusoidal load was performed. The mentioned analysis was conducted using software based on the finite element method. A comparative analysis of the plate with the different ply orientation (0°/90°/90°/0° and -45°/45°/45°/-45°) was done. The obtained results were analyzed and appropriate conclusions were made.

KEYWORDS

Laminated composite, Generalized Hooke's law, Finite element method, Bending analysis.

1. INTRODUCTION

Many elements of modern constructions require material characteristics that do not have conventional materials. Such requirements can only be met by composite materials (composites), which are a combination of two or more materials with different characteristics. The development of these materials stemmed primarily from the need to achieve the highest possible strength and rigidity in many structures while reducing weight. The advantage of composites over classic structural materials (metals) is that parts of the composite can be designed so that they can have different material properties in different cross-sections and different directions. Also, composite materials have high resistance to corrosion, material fatigue, good behavior in structural elements exposed to bending. Longer service life of composites reduces maintenance costs, on the one hand, and reduces exploitation costs due to the lower weight of structural elements, on the other hand. In addition to the above advantages, composite materials as well as other materials have their disadvantages. Due to the complexity of their structure (consist of two or more materials), it is often very difficult to diagnose damages at the internal structure of a composite material. Then, servicing and repairing structural elements made of composite materials can be much more difficult than constructions made of conventional materials, which ultimately increases maintenance costs. Delamination of laminated composites can occur due to the stress concentration at the contact of two layers with different material characteristics. This breaks the matrix and damages the laminate. Despite the mentioned disadvantages, having in mind all the above advantages, laminated composites are the current topic of research which is evidenced by a large number of review papers [1-4]. The static problems of bending and buckling of laminated plates for different cases of boundary conditions were analysed by the authors in the papers [5-7]. The influence of different ply orientation in square and rectangular laminated plates was studied for different cases of dynamic loading. In [8-10], free vibrations of laminated plates under different boundary conditions were studied. The propagation of elastic waves in laminated composite with special emphasis on Lamb waves was also analyzed [11-13]. In order to overcome delamination as the main disadvantage of laminated composites, in recent years the authors have been researching functionally graded materials [14-16].

2. CLASSIFICATION OF LAMINATED COMPOSITES

There are a large number of classification of composite plates with plies in the literature and there is no completely clear classification because they are such materials whose characteristics are under control of the designer. The type of composite plates with plies depends of the geometric parameters of the plate, the way that plies are combined, the material characteristics of the individual ply, etc.

Depending on the material of the constituents, the composite plates with plies can be:

1. **Sandwich composite plates or sandwich composites**
2. **Laminated composite plates or laminated composites**

Sandwich composites or laminates with core contains two outer plies and one middle ply that is usually made of cheaper and lighter material. In this way, the price is reduced but at the same time the bending stiffness of the laminate is improved.

Laminated composites, unlike sandwich laminates, do not have a core. Depending on whether they are plies consist of the same or different materials, their further classification is: homogeneous and hybrid laminated composites. Considering the way of defining sandwich laminates, it is completely clear that they can only be hybrid.

The other one classification of laminated composites is based on geometric parameters (angles of orientation of individual plies in relation to the adopted global coordinate system or in relation to the middle plane of the laminate, thickness of individual plies, mutual position of adjacent layers, etc.). The most general classification of laminated composites based on the geometric characteristics of the plies in relation to the middle plane is [17]:

1. **Symmetrical laminates**
2. **Antisymmetrical laminates**
3. **Asymmetrical laminates ili non-symmetrical laminates**

Symmetrical laminates (Figure 1a) - The geometric characteristics are symmetrical in relation to the middle plane of the plate. It means that the angles of orientation of the plies, the thickness of the plies and the characteristics of the material above and below the middle plane are equal to each other:

$$\theta(z)=\theta(-z),\ C^k_{ij}(z)=C^k_{ij}(-z),\ h_k(z)=h_k(-z), \tag{1}$$

where are:

z=0 - equation of middle plane,
θ - the orientation angle of the fibers in relation to the global coordinate system,
C^k_{ij} - coefficients of elasticity of the ply “k” in relation to the middle plane,
h_k - the thickness of the ply “k” in relation to the middle plane.

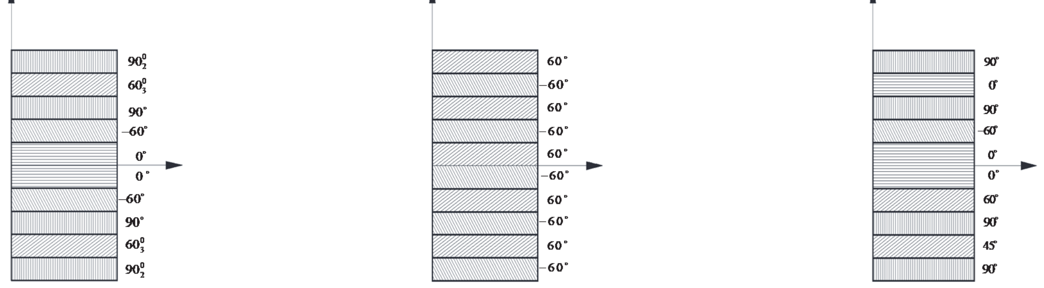

a) symmetrical laminates b) antisymmetrical laminates c) asymmetrical laminates

Figure 1: Laminated composite constituted of single-directional plies with different orientation

Antisymmetrical laminates (Figure 1b) - the plies thicknesses and material characteristics of the plies above and below the middle plane are equal to each other, while the angles of orientation of the fibers relative to the global coordinate system, above and below the middle plane, are opposite signs:

$$\theta(z)=-\theta(-z),\ C_{ij}^{k}(z)=C_{ij}^{k}(-z),\ h_k(z)=h_k(-z), \tag{2}$$

Asymmetrical laminates (Figure 1c) - there is a complete independence of the geometric characteristics of the plies above and below the middle plane, so a mathematical relationship cannot be established between the orientation angles, material characteristics and ply thickness above and below the middle plane.

Further, based on geometric characteristics, ie. based on the orientation of plies, laminates can be classificated as:

1. **Angle ply laminates**
2. **Cross ply laminates**
3. **Angle ply and cross ply laminates**
4. **Quasi-isotropic laminates**
5. **General laminates**

Angle ply and cross ply laminates have two orthogonal planes of symmetry which do not necessarily coincide with the planes of the adopted coordinate system. The directions of the plane of symmetry in relation to the adopted coordinate system are bisector directions, while the angle between of the bisector line and one of the axes of the coordinate system is the bisector angle▯▯. The fibers of individual plies are shifted relative to the bisector direction by laminate angles ±▯. The main difference between angle ply and cross ply laminates is: angle ply laminates can have arbitrary values of angles ▯▯and ±▯, while cross ply laminates have fixed value of the bisector and laminate angle (▯=45° and▯▯=±45°). For the value of the bisector angle ▯=0°, the directions of material symmetry and coordinate axes coincide.

Quasi-isotropic laminates are a type of laminate in which the plies are laid in such a way that the laminate acts as an isotropic ply under plane load.

Generalized laminates are laminates in which the plies can have completely different fiber orientations and analysis such laminates is difficult in terms of macromechanical properties.

Based on the thickness of the plies, it is possible to classificated the laminate as:

1. **Balanced laminates**
2. **Unbalanced laminates**

Balanced laminates - all plies must have the same thickness.

Unbalanced laminates - the thicknesses of the plies may be partially or completely different.

It should be emphasized that there are no clear boundaries between the previously listed tupes of laminates, so for example one laminate can be at same time symmetrical, quasi-isotropic and unbalanced. Therefore, in the literature often when describing macromechanical characteristics can be found, for example, symmetric quasi-isotropic laminates or non- symmetric cross ply laminates, etc.

3. GENERALIZED HOOK'S LAW

3.1. Coefficients of the constitutive matrix

The coefficients of constitutive matrix can be expressed by using:

1. Engineering constants
2. Elastic constants defined in Spencer's papers

Expressing the coefficients of the constitutive matrix by using engineering constants is a much more common, especially in engineering practice. Also, this way of expression is more suitable for application in numerical methods such as the finite element method. The second principle of expressing the coefficients of the constitutive matrix is useful due to its invariance in relation to the rotation of the coordinate system, so it is not necessary to use transformations of the constitutive matrix. Depending on the class of symmetry of the constituents, composite materials require the definition of a greater number of material constants then to conventional materials. Experimental static and dynamic methods are used to determine the material constants. Laminated composite are a type of composite material that consists of several individual fiber-reinforced plies of the same or different orientation. Plies can be composed of materials with different types of symmetry from isotropic to completely anisotropic and can have different structures, thicknesses and mechanical properties. The most common constituents of laminated composite are plies with the following classes of symmetry:

1. Isotropic
2. Transversely isotropic
3. Orthotropic
4. Anisotropic with monoclinic type of symmetry
5. Anisotropic with triclinic type of symmetry

When the laminate is constituted of fiber-reinforced materials, then the constituents of the laminate are most often orthotropic classes of symmetry. Coordinate system rotations can cause the ply symmetry class relative to the global coordinate system to correspond to anisotropic material with monoclinic symmetry type. Orthotropic single-directional composite layer are obtained as a combination of single-directional plies which have one privileged direction that coincides with one of the axes of the global coordinate system. Planes normal in that direction have isotropic characteristics. They represent the simplest structure of orthotropic materials and consist of single-directional layers whose material coordinates 1, 2 and 3 coincide with the coordinates of the layers x, z, y. Figure 2 shows layer with orthotropic type of material symmetry.

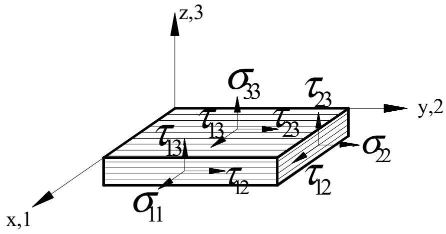

Figure 2: Layer with orthotropic type of material symmetry

Hook's generalized law for orthotropic type of material symmetry is:

$$\begin{Bmatrix} \sigma_{11} \\ \sigma_{22} \\ \sigma_{33} \\ \tau_{23} \\ \tau_{13} \\ \tau_{12} \end{Bmatrix} = \begin{bmatrix} \frac{1-\nu_{23}\nu_{32}}{E_2E_3\Delta} & \frac{\nu_{21}+\nu_{23}\nu_{31}}{E_2E_3\Delta} & \frac{\nu_{31}+\nu_{21}\nu_{32}}{E_2E_3\Delta} & 0 & 0 & 0 \\ \frac{\nu_{21}+\nu_{23}\nu_{31}}{E_2E_3\Delta} & \frac{1-\nu_{13}\nu_{31}}{E_1E_3\Delta} & \frac{\nu_{32}+\nu_{12}\nu_{31}}{E_1E_3\Delta} & 0 & 0 & 0 \\ \frac{\nu_{31}+\nu_{21}\nu_{32}}{E_2E_3\Delta} & \frac{\nu_{32}+\nu_{12}\nu_{31}}{E_1E_3\Delta} & \frac{1-\nu_{12}\nu_{21}}{E_1E_2\Delta} & 0 & 0 & 0 \\ 0 & 0 & 0 & G_{23} & 0 & 0 \\ 0 & 0 & 0 & 0 & G_{13} & 0 \\ 0 & 0 & 0 & 0 & 0 & G_{12} \end{bmatrix} \begin{Bmatrix} \varepsilon_{11} \\ \varepsilon_{22} \\ \varepsilon_{33} \\ \gamma_{23} \\ \gamma_{13} \\ \gamma_{12} \end{Bmatrix} \tag{3}$$

where is:

$$\Delta = \frac{\left(1-\nu_{12}\nu_{21}-\nu_{23}\nu_{32}-\nu_{13}\nu_{31}-2\nu_{21}\nu_{32}\nu_{13}\right)}{E_1E_2E_3}. \tag{4}$$

In the case of small thickness orthotropic ply as a constituent of laminate, assuming plane type of stress state as well as that the displacement normal to plane of plate is constant, it can be neglect the third type and third column of the constitutive matrix, so equation (3) reduces to:

$$\begin{Bmatrix} \sigma_{11} \\ \sigma_{22} \\ \tau_{23} \\ \tau_{13} \\ \tau_{12} \end{Bmatrix} = \begin{bmatrix} \frac{1}{E_2\Delta} & \frac{\nu_{21}}{E_2\Delta} & 0 & 0 & 0 \\ \frac{\nu_{21}}{E_2\Delta} & \frac{1}{E_1\Delta} & 0 & 0 & 0 \\ 0 & 0 & G_{23} & 0 & 0 \\ 0 & 0 & 0 & G_{13} & 0 \\ 0 & 0 & 0 & 0 & G_{12} \end{bmatrix} \begin{Bmatrix} \varepsilon_{11} \\ \varepsilon_{22} \\ \gamma_{23} \\ \gamma_{13} \\ \gamma_{12} \end{Bmatrix} \tag{5}$$

where is:

$$\Delta = \frac{(1-\nu_{12}\nu_{21})}{E_1 E_2}. \tag{6}$$

4. FINITE ELEMENT MODELLING OF LAMINATED COMPOSITE

In most cases when the analyzed structural element has a complex geometry, complex load and different materials, it is not possible to find a solution in analytical form. Analytical solution involves obtaining analytical expressions for calculating the required quantities at different points (stress, deformation, temperature, etc.). To obtain such data, it is necessary to solve differential [18] or partial differential equations, which can only be done for very simple problems. Therefore, numerical methods are used. One of the most commonly used numerical method is finite element method (FEM). The development of computer technology has led to the expansion of the use of numerical methods, so that today numerical analysis is often a mandatory part of project documentation. The use of numerical methods can achieve significant savings in economic terms, especially in structures where it is not necessary to perform experiments.

4.1. Description of model

A laminated composite plate fixed along all four edges and loaded with a sinusoidally distributed load was analyzed (Figure 3):

$$q(x,y) = q_0 \sin\left(\frac{\pi x}{a}\right)\cos\left(\frac{\pi y}{b}\right). \tag{7}$$

The geometric and material characteristics of the composite plate are given (8). Static analysis was performed for two cases of ply orientation of symmetrical cross ply laminate (0°/90°/90°/0° и -45°/+45°/+45°/-45°) by using the finite element method. The FE model is discretized with 1024 finite elements and 1089 nodes.

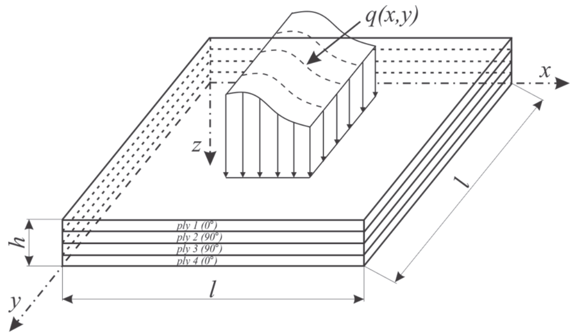

a) symmetrical cross ply laminate 0°/90°/90°/0°

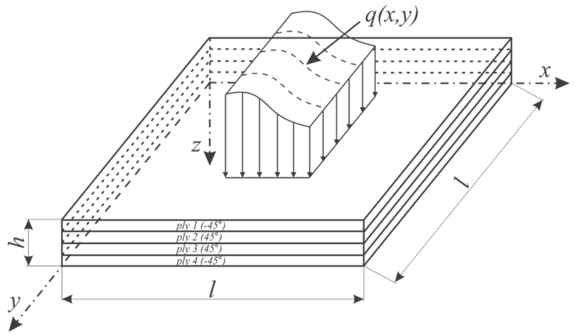

b) symmetrical cross ply laminate -45°/+45°/+45°/-45°

Figure 3: Laminated composite plates under sinusoidally distributed load

Geometric and material characteristics of laminated composite plate are:

$$\begin{aligned} & h = 0.24\,cm; \qquad l = 12\,cm; \\ & E_1 = 174.6\cdot 10^5\,\frac{N}{cm^2}; \qquad E_2 = 7\cdot 10^5\,\frac{N}{cm^2} \\ & G_{12} = 3.5\cdot 10^5\,\frac{N}{cm^2}; \qquad G_{1z} = 3.5\cdot 10^5\,\frac{N}{cm^2}; \qquad G_{2z} = 1.4\cdot 10^5\,\frac{N}{cm^2} \\ & \nu_{12} = 0.25 \end{aligned} \tag{8}$$

4.2. Numerical results

Bending analysis of plate for two different cases of ply orientation was performed. In order to perform a comparative analysis of the obtained values of displacement and stress, the mentioned values are normalized according to:

$$\bar{w} = \frac{100E_2h^3}{q_0l^4}w\left(\frac{l}{2},\frac{l}{2}\right); \quad \bar{\sigma}_{xx}(z) = \frac{h^2}{q_0l^2}\sigma_{xx}\left(\frac{l}{2},\frac{l}{2},z\right); \quad \bar{\sigma}_{yy}(z) = \frac{h^2}{q_0l^2}\sigma_{yy}\left(\frac{l}{2},\frac{l}{2},z\right); \quad \bar{\tau}_{xy}(z) = \frac{h^2}{q_0l^2}\tau_{xy}(z). \tag{9}$$

Table 1 shows the comparative results of normalized values of vertical displacement $\bar{w}$, normal stresses $\bar{\sigma}_{xx}$, $\bar{\sigma}_{yy}$ and shear stress $\bar{\tau}_{xy}$ for symmetrical cross ply laminate with two different combinations of ply orientation.

Table 1: Normalized values of vertical displacement $\bar{w}$, normal stresses $\bar{\sigma}_{xx}$, $\bar{\sigma}_{yy}$ and shear stress $\bar{\tau}_{xy}$

Ply orientation	w	σ_{xx}				σ_{yy}				τ_{xy}			
		ply 1	ply 2	ply 3	ply 4	ply 1	ply 2	ply 3	ply 4	ply 1	ply 2	ply 3	ply 4
0°/90°/90°/0°	0.1213	-0.1620	-0.0552	0.0552	0.1620	-0.0082	-0.0027	0.0027	0.0082	0.0038	-0.0013	0.0013	-0.0038
-45°/45°/45°/-45°	0.1484	-0.1470	-0.0835	0.0835	0.1470	-0.0114	-0.0028	0.0028	0.0114	-0.0092	0.0031	-0.0031	0.0092

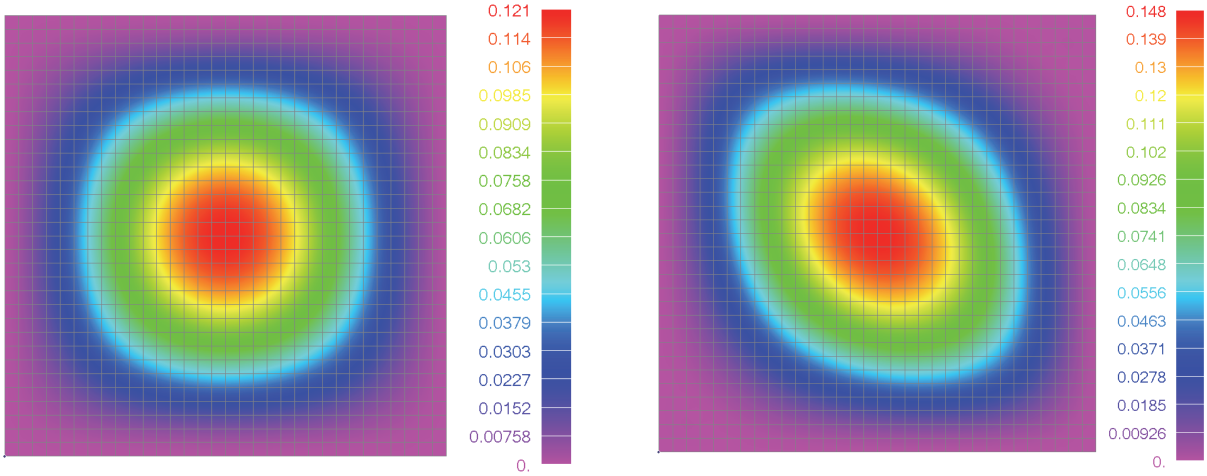

a) symmetrical cross ply laminate 0°/90°/90°/0°

b) symmetrical cross ply laminate -45°/+45°/+45°/-45°

Figure 4: Normalized values of vertical displacement field $\bar{w}$

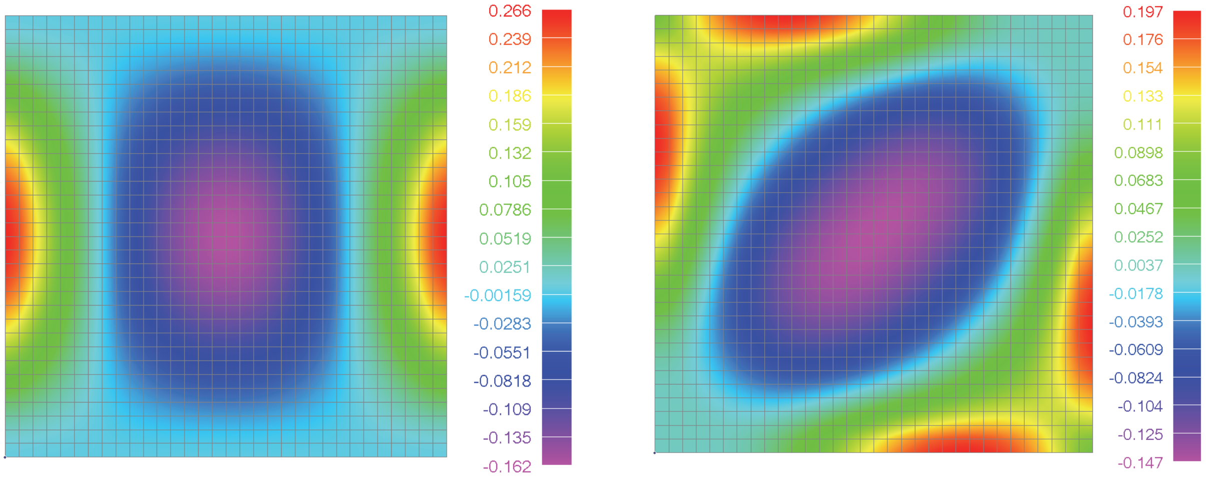

a) symmetrical cross ply laminate 0°/90°/90°/0°

b) symmetrical cross ply laminate -45°/+45°/+45°/-45°

Figure 5: Normalized values of normal stress field $\bar{\sigma}_{xx}$ - ply 1

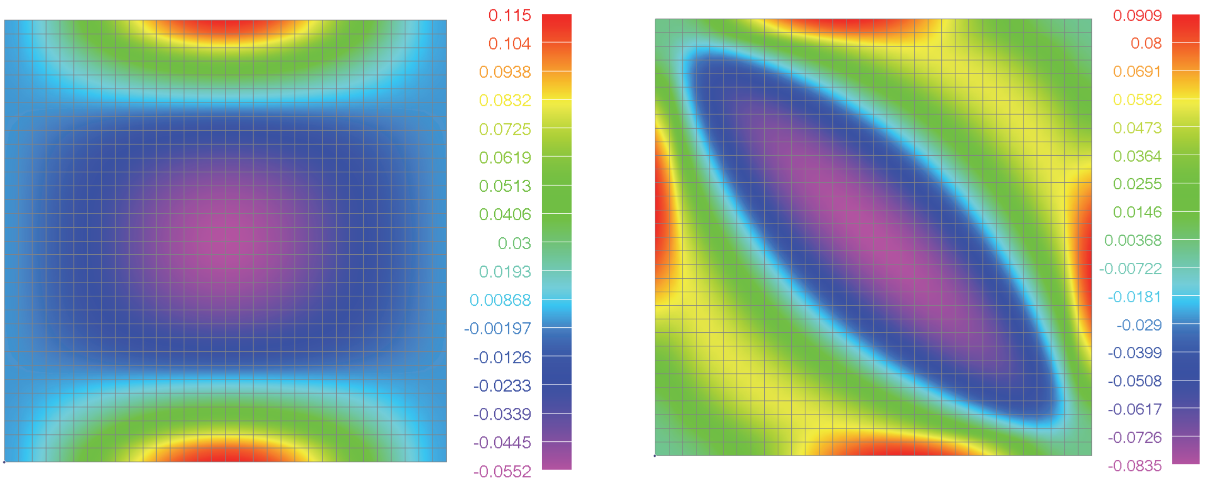

a) symmetrical cross ply laminate 0°/90°/90°/0°

b) symmetrical cross ply laminate -45°/+45°/+45°/-45°

Figure 6: Normalized values of normal stress field $\bar{\sigma}_{xx}$ - ply 2

By analyzing the obtained results, it can be concluded that a higher value of vertical displacement was obtained for the laminated plate with the ply orientation -45°/45°/45°/-45° compared to laminated plate with the ply orientation is 0°/90°/90°/0°. The value of the maximum displacement of the center point on the plate is about 20% higher in the second case compared to the first case of ply orientation. When we analyze the stresses, different values of normal and shear stresses in different layers are obtained. For example, the normal stresses and shear stress are about 3 times higher in ply 1 compared to ply 2 for plate with 0°/90°/90°/0° ply orientation. The same relation is in ply 4 compared to ply 3. Precisely different values of certain stresses in different plies can serve as a starting point in the design phase of laminated structural elements. By a different combination of the orientation of the plies, the desired strength and rigidity of the designed structural element can be achieved. The influence of the different ply orientation of the laminated plate to the values of displacement and stresses can best be seen in Figures 4-6. Figure 4 shows the normalized values of vertical displacement field $\bar{w}$ of the laminated plate while normalized values of normal stress field $\bar{\sigma}_{xx}$ in ply 1 and 2 are presented in Figure 5 and Figure 6.

5. CONCLUSIONS

This paper points out the importance of research and use of composite materials with special emphasis on laminated composite materials. A brief overview of the current state of research related to mentioned area is given. Particular accent is placed on the basic advantages and disadvantages of composite materials compared to conventional materials. The classification of laminated composites from the aspect of different criteria is presented. The relations between stress and strain in the field of linear elasticity is given by the generalized Hooke's law. The constitutive matrix for the orthotropic class of material symmetry are expressed by engineering constants. Finally, a comparative bending analysis of two laminated composite plates with different ply orientations was performed by using finite element methods. Comparative results of vertical displacement and stresses for the cases of symmetrical cross ply laminate 0°/90°/90°/0° and symmetrical cross ply laminate -45°/45°/45°/-45° are shown. By analyzing the results, it was noticed that higher vertical displacement of central point at plate is obtained in the case of the ply orientation -45°/45°/45°/-45° compared to the laminated plate with the ply orientation 0°/90°/90°/0°.

ACKNOWLEDGEMENTS

Research presented in this paper was supported by Ministry of Education, Science and Technological Development of Republic of Serbia, Grant TR33015, TR32036 and multidisciplinary project III 44007.

REFERENCES

[1] V. Birmana and G. A. Kardomateas, "Review of current trends in research and applications of sandwich structures", Compos. Part B, Vol. 142, pp. 221-240, https://doi.org/10.1016/j.compositesb.2018.01.027, (2018)

[2] K.M. Liew, Z.Z. Pan and L.W. Zhang, "An overview of layerwise theories for composite laminates and structures: Development, numerical implementation and application", Compos. Struct, Vol. 216, pp. 240-259, https://doi.org/10.1016/j.compstruct.2019.02.074, (2019)

[3] J. Galos, "Thin-ply composite laminates: a review", Compos. Struct, Vol. 236, p. 111920, https://doi.org/10.1016/j.compstruct.2020.111920 ,(2020)

[4] Q. Guo, W. Yao, W. Li and N. Gupta, "Constitutive models for the structural analysis of composite materials for the finite element analysis: A review of recent practices", Compos. Struct, Vol. 260, p. 113267, https://doi.org/10.1016/j.compstruct.2020.113267, (2021)

[5] N. Garg, N. D. Chakladar, B. G. Prusty, C. Song and A. W. Phillips, "Modelling of laminated composite plates with weakly bonded interfaces using scaled boundary finite element method," Int. J. Mech. Sci, Vol. 170, p. 105349, https://doi.org/10.1016/j.ijmecsci.2019.105349, (2020)

[6] Z. Ullah, Ł. Kaczmarczyk, X.-Y. Zhou, B.G. Falzon and C.J. Pearce, "Review of current trends in research and applications of sandwich structures", Compos. Part B, Vol. 201, p. 108321, https://doi.org/10.1016/j.compositesb.2020.108321, (2020)

[7] A. Radaković, D. Čukanović, D. Milosavljević, G. Bogdanović and S. Husović, "New shape function in buckling analysis of composite laminates used in transport vehicles", Proceedings of 8th International Congress Motor Vehicles & Motors 2020, "ECOLOGY-VEHICLE AND ROAD SAFETY - EFFICIENCY", Faculty of Engineering, University of Kragujevac, Kragujevac (Serbia), 8-9 October 2020, pp. 169-174, (2020)

[8] A. Bendahmane, S. M. Hamza-Cherif, and M. N. Ouissi, “Free vibration analysis of variable stiffness composite laminate (VSCL) plates coupled with fluid”, Mech. Adv. Mater. Struc, Vol. 28, pp. 167-181, https://doi.org/10.1080/15376494.2018.1553257, (2021)

[9] M. A. Benhenni, B. Adim, T. H. Daouadji, B. Abbès, F. Abbès, Y. Li and A. Bouzidane, “A Comparison of Closed-Form and Finite-Element Solutions for the Free Vibration of Hybrid Cross-Ply Laminated Plates”, Mech. Compos. Mater,” Vol. 55, pp. 181-194, https://doi.org/10.1007/s11029-019-09803-2, (2019)

[10] D. Milosavljević, A. Radaković, D. Čukanović, G. Bogdanović and S. Husović, “New shape function in the free-vibration analysis of antisymmetric crossply composite laminates”, Scientific Publications of the State University of Novi Pazar, Series A: Applied Mathematics, Informatics & Mechanics, Vol. 13, pp. 27-42, (2021)

[11] O. Saito, F. Yu and Y. Okabe, “Dispersion relation of Lamb waves in cross-ply composite laminates using multi-layered models”, Compos. Struct, Vol. 264, p. 113691, https://doi.org/10.1016/j.compstruct.2021.113691,(2021)

[12] A. Radaković, G. Bogdanović, D. Milosavljević, Lj. Veljović and D. Čukanović, “Using high-order shear deformation theory in the analysis of Lamb’s waves propagation in materials reinforced with two families of fibers”, Acta Mech, Vol 228, pp. 187-200, https://doi.org/10.1007/s00707-016-1707-1, (2017).

[13] G. Bogdanović, D. Milosavljević, A Radaković, D. Čukanović and V. Geroski, “Acoustical tensor and elastic wave propagation in anisotropic materials used in automotive industy s”, Mobility & Vehicle Mechanics, Vol 43, pp. 63-71, https://doi.org/10.24874/mvm.2017.43.03.05, (2017)

[14] S. Thai, V. X. Nguyen and Q. X. Lieu, “Bending and free vibration analyses of multi-directional functionally graded plates in thermal environment: A three-dimensional Isogeometric Analysis approach”, Compos. Struct, Vol. 295, p. 115797, https://doi.org/10.1016/j.compstruct.2022.115797, (2022)

[15] A. Radaković, D. Čukanović, G. Bogdanović, M. Blagojević, B. Stojanović, D. Dragović and N. Manić, “Thermal Buckling and Free Vibration Analysis of Functionally Graded Plate Resting on an Elastic Foundation According to High Order Shear Deformation Theory Based on New Shape Function”, App. Sci, Vol. 10, p. 4190, https://doi.org/10.3390/app10124190 , (2020)

[16] D. Čukanović, A. Radaković, G. Bogdanović, M. Milanović, H. Redžović and D. Dragović, “New Shape Function for the Bending Analysis of Functionally Graded Plate, Materials”, Vol. 11, p. 2381, https://doi.org/10.3390/ma11122381 , (2018)

[17] A. Radaković, “Primena smicajnih deformacionih teorija viseg reda u makromehanickoj analizi kompozitnih laminata”, PhD Thesis, Univerzitet u Kragujevcu, Fakultet inženjerskih nauka, (Serbia), (2015).

[18] S. Kostić, N. Vasović and J. Trivan, “Sensitivity of a Simple Earthquake Nucleation Model to Small Parameter Perturbation: Conditions for the Occurrence of Deterministic Chaos”, Vol. 1, pp. 27-33, (2022)

ORIGINAL SCIENTIFIC PAPER OPEN ACCESS

Analysis of the hydraulic binder use for base strengthening in pavement constructions

Miloš Šešlija[1*], Igor Peško[1], Katarina Mirković[2], Vladimir Mandić[3], Fawzia Kired[1]

[1] University of Novi Sad, Faculty of Technical Sciences, Novi Sad, Serbia

[2] University of Podgorica, Faculty of Civil Engineering, Podgorica, Montenegro

[3] University of Kragujevac, Faculty of Mechanical and Civil Engineering, Kraljevo, Serbia

ARTICLE INFO

* **Correspondence:** sele@uns.ac.rs

DOI: 10.5937/engtoday2202037S

UDC: 621(497.11) **ISSN:** 2812-9474

Article history: Received 27 June 2022; Accepted 11 July 2022

ABSTRACT

The paper presents the application of cement stabilization in the world and in our country. In addition to the literature review, basic physical - mechanical tests of the pavement base without the use of hydraulic binder and with the use of hydraulic binder with different percentages of participation (3, 5, and 7%) were given. The hydraulic binder of the manufacturer LaFarge HRB 12.5 was used as a binder, and the material on which this binder was tested is a clay material taken from Subotica. Using this binder, it was concluded that any percentage of binder leads to significant improvement of the placenta and thus improves the load-bearing capacity of the pavement structure.

KEYWORDS

Hydraulic binder, Base, Pavement construction

1. INTRODUCTION

During the infrastructure building, it is sometimes impossible to avoid sections where the foundation soil or pavement base soil does not meet the minimum requirements, either in terms of load-bearing capacity or in terms of required material quality, and which the project or some general applicable regulation imposes on the material itself and its installation condition. There are several procedures, groups of soil stabilization procedures: mechanical, stabilization with lime, cement or similar hydraulic binders, bituminous binders, special chemical agents and geotextiles.

The basic mechanism for mechanical soil stabilization is thickening, then its granulometric composition must be improved. When soil stabilization is carried out with binders, hardening is achieved by connecting soil particles by mixing with binders. Necessary groups are soil stabilization procedures using geotextiles, when geotextiles (non-woven textiles, mesh) and a layer of stone material are laid over weak and unstable soil, which is used to establish the required load-bearing capacity.

The first application of soil stabilization was achieved approximately 5000 years ago, when the so-called Shaanxi-pyramids (towards the province of Shaanxi) were made of clay mixed with lime. The Chinese wall between the brick walls has a core of clay stabilized with lime, and the Chinese used the same procedure to build roads and improve the soil during the bridges building. The Indians used a mixture of clay and lime as masonry mortar, and the Romans built roads with lime and volcanic ash 2000 years ago.

The Roman road Via Appia has three of the four layers of pavement structure (1.2 m thick) stabilized with lime. The practice of stabilizing the soil with hydraulic binders (lime, pozzolan) in many countries has survived to our time. Modern soil stabilization procedures, which are based not only on experience but also on professional and scientific claims, began to develop first in the United States. Due to the very bad condition of the roads at the beginning of our century and the need to connect very remote areas, various possibilities of soil consolidation were begun to be studied.

The national reports of the World Congress on Roads (AIPCR) show that four basic stabilization procedures are applied today (mechanical, lime, hydraulic binders, bitumen) and that they have become standard techniques in more than 50 countries. The mentioned stabilization procedures have also been applied in our country since the 1960s. They are mostly standardized by SRPS standards. Stabilization, improvement of bearing capacity with the help of geotextiles, began to be applied much later (around 1960), which was conditioned by the ability of the industry to produce sufficient quantities of these materials, at low enough prices, to be rationally used in construction.

The papers encountered in the last decade are the stabilization of fine-grained soil with fly ash [1]. The authors examined low to medium plasticity clay as well as medium to high plasticity clay. The ash was used as a binder in the amount of 15 to 20%. After the tests, it is concluded that the ash can be used to improve the pavement base. Some of the authors have examined the use of ash as a material for the construction of road embankments using a hydraulic binder (lime and cement) with different percentages [2]. The authors came to the conclusion that the application of ash with or without binders can be used for road construction and give quite good test results. Some authors have examined river sludge as bedding material in pavement bases. As a binder, they used cement with the addition of ash up to 20%, on the basis of which they concluded that ash and sludge can be used as embankments of material [3]. Many papers are related to the use of waste and recycled materials [4-9] for the production of pavement layers and with the addition of binders in order to improve the load-bearing capacity in the layer.

This paper presents the basic physical and mechanical tests of the pavement base with and without the addition of binders, in order to be able to compare the values and show how much the hydraulic binder has improved in terms of natural soil characteristics. As a binder, a hydraulic binder was used, which was formed by a combination of lime and cement. The percentages of soil stabilizer binder additives are 3, 5 and 7%.

2. MATERIALS

Natural material (clay material) and hydraulic binder (BeoBond C30 "LaFarge" from Beocin) were used to make the stabilized pavement base. The location of the taken sample is shown in Figure 1.

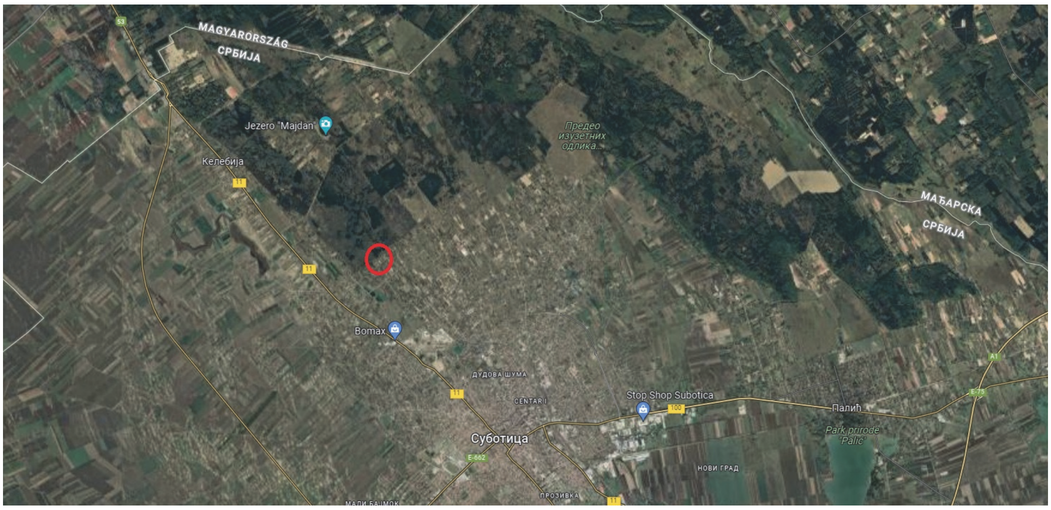

Figure 1: View of the location of the taken material sample

2.1. Clay material of low plasticity

To test this type of soil, tests were performed according to the following standards:

- determination of granulometric composition of aggregates (SRPS U.B1.018: 2005 [10], SRPS EN 933-1: 2013 [11]),
- determination of soil sample moisture (SRPS U.B1.012: 1995 [12]),
- determination of soil consistency, Atterberg limits (SRPS U.B1.020: 1980 [13]),
- determination of the ratio of moisture and dry bulk density of soil (SRPS EN 13286-2: 2012 [14]),
- determination of the California load index (SRPS EN 13286-47: 2012 [15]).

2.1.1. Granulometric composition

In order to classify the material, the granulometric composition and distribution of particles as a function of grain size were examined. The method of wet sowing with the use of distilled water was applied. To determine the granulometric composition of the clay, 300 g of material with a series of sieves were used: 4, 2, 1 mm and 500, 250, 125, 90, 63 μm. Most of the material passed through a 1 mm sieve (77%), with rare exceptions. A total of 1 sample was made, in accordance with the appropriate standards, and depending on the size of the tested particles:

- SRPS EN 933 - 1: 2013 - Tests for particle size distribution of aggregates - Part 1: Determination of particle size distribution - Screening method,
- SRPS U.B1.018: 2005 - Geomechanical testing: Determination of particle size distribution.

The tested sample can be classified into a group of very fine clay materials. The granulometric composition of the aggregate is given in Figure 2.

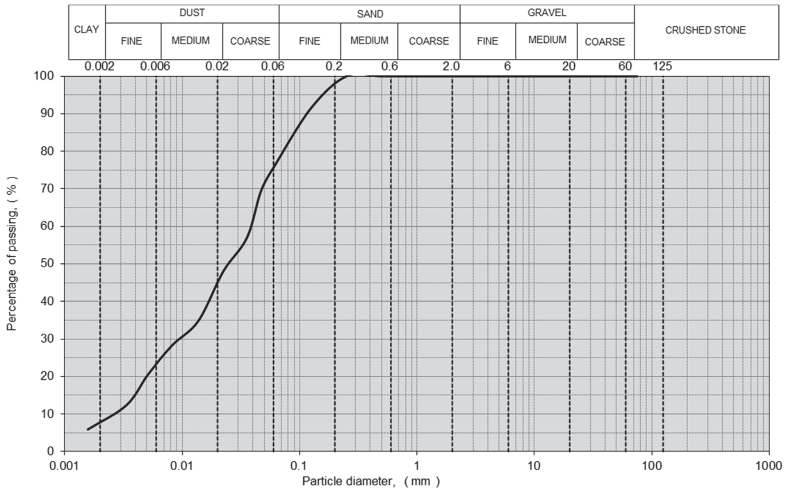

Figure 2: Granulometric composition of aggregates

According to the USCS [16] classification, the material belongs to the CL group or low plasticity clay, while according to the AASHTO [17] classification it belongs to the A-7-6 group, ie it belongs to the group with high plasticity index in relation to their yield strengths, and such materials can be highly elastic and subject to significant changes in volume.

2.1.2. Material compaction characteristics (Proctor`s experiment)

This procedure defines the optimal water content. With it the largest dry bulk density is achieved, with the applied compaction energy, and under the conditions defined by the standard:

- SRPS EN 13286-2: 2012 - Unbound and hydraulically bound mixtures - Part 2: Test methods for laboratory reference volume and water content - Proctor compaction.

In accordance with the granulometric composition, a compaction energy of 600 kN/m3 was applied, and under the assumption that the same will be applied in the field. The test results of the Proctor test are shown in Figure 3. It is observed that the maximum bulk density is 1.61 t/m^3 at an optimum humidity of 20.1%.

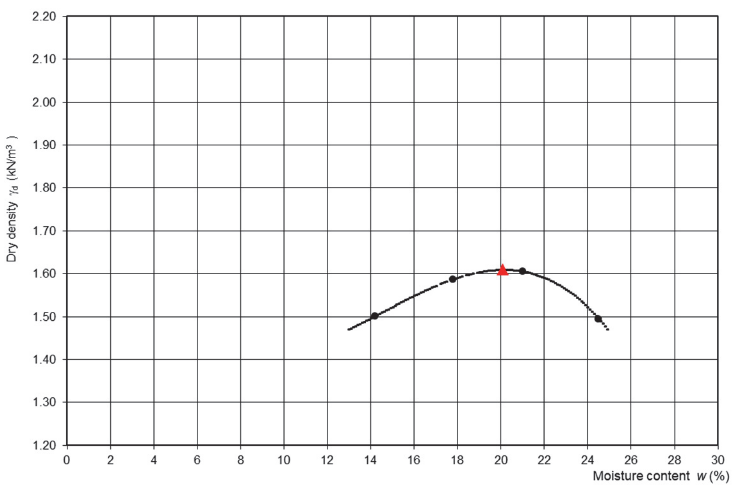

Figure 3: Chart of Proctor's test

2.1.3. Load-bearing capacity of the California load-bearing index

The California Load Index (CBR) is a number that physically represents the resistance of a standard piston to standard values. When designing pavement structures in road construction, one of the basic parameters of material quality, and in the technical conditions of construction, is prescribed as a mandatory parameter in the production of bedding. The experiment was performed according to the procedure and in the apparatus, with accessories and measuring devices that are clearly defined by the standard:

- Unbound and hydraulically bound mixtures - Part 47: Test methods for the determination of California bearing capacity index, immediate bearing capacity index and linear swelling.

After the test, the CBR value for penetration of 2.54 mm is 6.3%, while for penetration of 5.08 mm is 5.29%. In Figure 4 show the diagram of CBR.

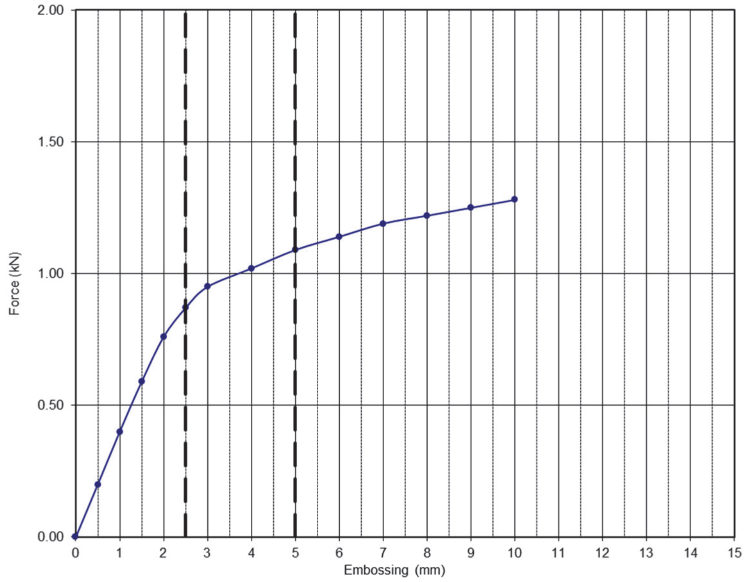

Figure 4: Diagram of CBR

2.2. BeoBond C30 “LaFarge” Beočin

The following tests were performed for testing the hydraulic road binder:

- start and end of binding time - SRPS EN 196-3 [18],
- standard consistency SRPS EN 196-3 [18],
- volume constancy (Le Chatelier rings) SRPS EN 196-3 [18],
- determination of compressive strength of cement after 7 and 28 days SRPS EN 196-1 [19],
- determination of flexural strength of cement after 7 and 28 days SRPS EN 196-1 [19].

The test results of this binder as well as the manufacturer's specifications or specifications of quality conditions prescribed by the standard SRPS EN 13282-2 are shown in Table 1.

Table 1: Results of laboratory tests of hydraulic road binder BeoBond C30 „LaFarge“ Beočin

Binder characteristics	Test results	Quality conditions [20]
Start of binding time (min) [18]	180	≥ 150
End of binding time (min) [18]	215	
Standard consistency (%) [18]	37.5	
Constancy of volume (Le Chatelier rings) (mm) [18]	0.33	≤ 10
Determination of compressive strength of cement after 7 days (MPa) [19]	18.1	
Determination of compressive strength of cement after 28 days (MPa) [19]	45.8	32.5-52.5
Determination of flexural strength of cement after 7 days (MPa) [19]	9.8	
Determination of flexural strength of cement after 28 days (MPa) [19]	10.7	

After the tests, it is concluded that the hydraulic road binder BeoBond C30 "LaFarge" Beočin fulfills the prescribed requirements defined by the standard SRPS EN 13282-2 [14].

3. ANALYSIS OF RESULTS AND DISCUSSION

The mixtures made in this paper are as follows:

- reference sample without added binder,
- sample with 3% binder,
- sample with 5% binder and
- sample with 7% binder.

The tests were performed according to the requirements of the standard SRPS EN 14227-11, which include the following tests:

- determination of optimal humidity and maximum bulk density - Proctor's test with 3, 5 and 7% binder,
- determination of the California load index after 30 minutes, 4 and 28 days of immersion in water,
- determination of compressive strength after 7 and 28 days.

In addition to the above tests prescribed by the standard [20], the following tests were additionally performed:

- determination of Atterberg`s consistency limits after 5, 15 and 30 minutes, with the addition of 3, 5 and 7% binder.

From the analyzed location, it was concluded that this is a material belonging to the group of low plastic clay (CL) according to the USCS classification of materials, which has certain yield limits W_L=42% and with a plasticity limit W_P=14%. The average humidity of the homogenized material is 28%. According to the AASHTO classification, the material belongs to group A-7-6.

Figures 5 and 6 show the changes in the yield strength W_L, the plasticity limit W_P as well as the calculated plasticity index depending on the percentage of added binder over a period of 5, 15 and 30 minutes.

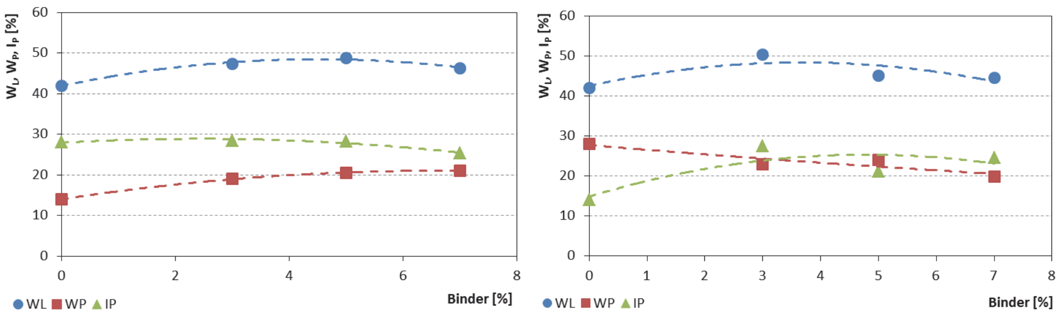

Figure 5: Change in Atterberg`s limits of consistency for the function of added lime after 5 minutes (left figure), after 15 minute (right figure)

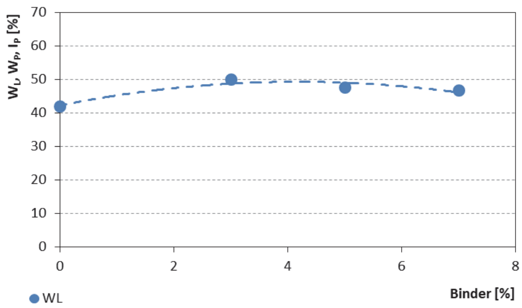

Figure 6: Change in Atterberg`s limits of consistency for the function of added lime after 30 minutes (left figure)

The change in the yield strength is negligible and ranges from 40 to 50%, and the plasticity limit increases from 14 to 28%, with a maximum value of 28% being achieved with 0% binder addition. The plasticity index decreases with increasing amount of binder. The minimum value of the plasticity index was achieved with 28.3% with a share of 5% binder. The plastic limit could not be determined 30 minutes after the addition of the binder at different participation values.

Figures 7 and 8 shows the flows of change in yield strength, plasticity as well as changes in the calculated plasticity index as a function of time.

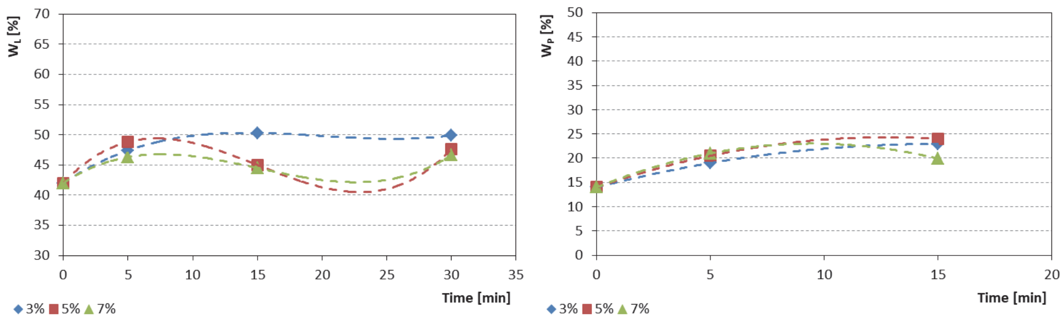

Figure 7: Change in the flow rate limits for the function of time for different percentages of added binder (left figure); change in the plasticity limits for the function of time for different percentages od added binder (right figure)

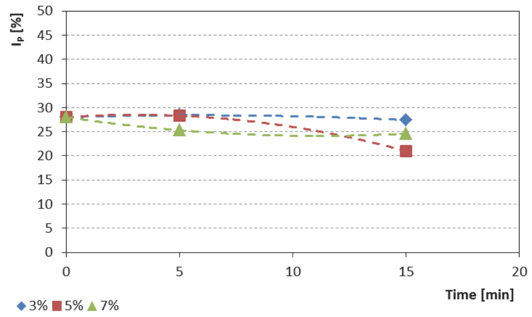

Figure 8: Change in the index of plasticity for the function of time for different percentages of added binder

The materials have reduced yield and plasticity limits, and there is not much difference in the achieved minimum value of the plasticity index with 3 and 5% of the binder addition.

The California load index was tested on the samples after 30 minutes, after 4 and 28 days of immersion in water. Table 2 shows the CBR values for a given time period.

Table 2: CBR values for a given time period

Binder (%)	after 30 minute		after 4 days		after 28 days	
	Direct loading capacity index	Category	Direct loading capacity index	Category	Direct loading capacity index	Category
3	29	IPL25	63.8	CBR50	88	CBR50
5	27	IPL25	71.9	CBR50	>100	CBR50
7	22	IPL20	67.7	CBR50	94.8	CBR50

The immediate load index, which was determined 30 minutes after the construction of the test body, belongs to the IPL25 category with 3 and 5% of binder, and the IPL20 category with 7% binder. CBR values determined after 4 days of immersion in water from the test body and results, belong to the CBR50 category with 3, 5 and 7% binder. No swelling of the material was registered on the test samples that were tested after 4 and 28 days of immersion in water for all three cases of the percentage of binder participation.

Compressive strengths after 7 and 28 days are shown in Table 3.

Table 3: Hardness values for pressure

Binder (%)	Rc, 7 (MPa)	Rc, 28 (MPa)	Category
3	-	0.75	Rc 0.5
5	0.481	1.23	Rc 1.0
7	1.25	1.78	Rc 1.0

Compressive strength values with 5 and 7% of binder reach the last value of the maximum category according to the requirements of the prescribed standard SRPS EN 14227-11, which is Rc 1.0 and which guarantees the achievement of permanent strength parameters.

Figure 9 shows the change in optimal humidity and maximum bulk density of the material depending on the percentage of added binder. As the percentage of binder increases, the optimum moisture content of the material increases and the maximum bulk density decreases.

The optimum moisture content of the material with 5% of binder increased by 1%, and the bulk density decreased from 1.61 to 1.56 g/cm^3.

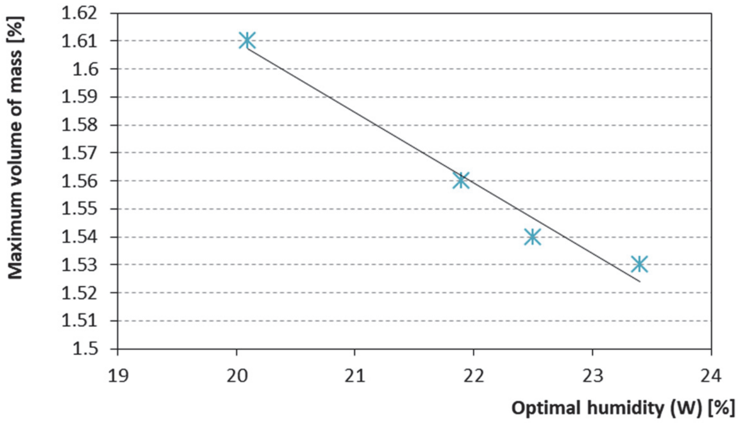

Figure 9: Change of the maximum volume of mass for the function of optimal humidity of the material for different percentage of added connective tissue

4. CONCLUSION

According to the conducted tests, the following can be stated:

- for more efficient installation of materials in the layers of the pavement construction, in terms of achieving the necessary parameters for material compaction, a percentage of 5 and 7% binder is recommended,
- with a percentage of 3% binder it is considered that the compressive strength would decrease by 20%, while the best values are achieved with a 7% binder addition using the standard [20],
- to achieve maximum effects in terms of load-bearing capacity, compaction and all analyzed segments from this paper, it is necessary to use a percentage of 5% binder,
- using a percentage of 3% or more percentage of binder during preparation will not cause swelling of the material, which accelerates enough that the binder quite quickly regulates the water in the layer.

ACKNOWLEDGEMENTS

This research (paper) has been supported by the Ministry of Education, Science and Technological Development through project no. 451-03-68/2022-14/ 200156 “Innovative scientific and artistic research from the FTS (activity) domain”.

REFERENCES

[1] M. Vukićević, V. Pujević, M. Marjanović, S. Jocković and S. Maraš-Dragojević, “Stabilization of fine-grained soils with fly ash”, Građevinar, Vol. 67, No. 8, pp. 761-770, https://doi.org/10.14256/JCE.1281.2014, (2015)

[2] M. Šešlija, N. Radović, M. Vasić, M. Đogo and M. Jotić: “Physico-mechanical properties of lfy ash applicable in road construction”, Građevinar, Vol.- 69, No. 10, pp. 923-932, https://doi.org/10.14256/JCE.1860.2016, (2016)

[3] D. Nakić, D. Voku, N. Štrimer and M. Serdar: “Management of sewage sludge-new possibilities involving partial cement replacement”, Građevinar, Vol. 70, No. 4, pp. 277-286, https://doi.org/10.14256/JCE.2164.2017, (2017)

[4] M. Zagvozda, S. Dimter, T. Rukavina and I. Netinger-Gubeša:”Possibilities of bioash application in road building”, Građevinar, Vol. 70, No. 5, pp. 393-402, https://doi.org/10.14256/JCE.2074.2017, (2018)

[5] M. Stojanović, V. Radonjanin, M. Malešev, T. Milović and S. Furgan: “Compressive strength of cement stabilizations containing recycled and waste materials”, Građevinar, Vol. 73, No. 8, pp. 791-804, https://doi.org/10.14256/JCE.3161.2021, (2021)

[6] Ž. Lebo, M. Bačić, D. Jurić-Kaćunić and M.S. Kovačević: “Zagreb clay improved with varioius binders”, Građevinar, Vol. 73, No. 9, pp. 871-880, https://doi.org/10.14256/JCE.3300.2021, (2021)

[7] R. Tanzadeh, M. Vafaeian and M. Y. Fard:"The Influence of lime powder on the behaviour of clay soil", Građevinar, Vol. 73, No. 9, pp. 907-915, https://doi.org/10.14256/JCE.1871.2016, (2021)

[8] Z. Zimar, D. Robert, A. Zhou, F. Giustozzi, S. Setunge and J. Kodikara: "Application of coal fly ash in pavement subgrade stabilisation: A review", Journal of Environmental Management, 312, pp. 1-18, https://doi.org/10.1016/j.jenvman.2022.114926, (2022)

[9] M. Zhang, M. Na, Z. Yang, Y. Shi, M. Guerrieri and Z. Pan: "Study on mechanical properties and solidification mechanism of stabilized dredged materijals with recycled GFRP fibre reinforced geopolymer", Case Studies in Construction Materials, Vol. 17, pp. 1-12, https://doi.org/10.1016/j.cscm.2022.e01187, (2022)

[10] SRPS U.B1.018 – Testing of soils. Determination of particle size distribution, (2005)

[11] SRPS EN 933-1 – Tests for geometrical properties of aggregates – Part 1: Determination of particle size distribution – Sieving method, (2009)

[12] SRPS U.B1.012 – Testing of soils. Determination of soil moisture content, (1995)

[13] SRPS U.B1.020 – Testing of soils. Determination of Atterberg limits, (1980)

[14] SRPS EN 13286-2 – Unbound and hydraulically bound mixtures – Part 2: Test methods for laboratory reference density and water content – Proctor compaction, (2013)

[15] SRPS EN 13286-47 – Unbound and hydraulically bound mixtures – Part 47: Test method for the determination of California bearing ratio, immediate bearing index and linear swelling, (2012)

[16] SRPS U.B1.001 – General classification of soils for engineering purposes, (1990)

[17] SRPS U.B1.002 – Testing of soils – Classification of soil and soil – aggregate mixtures for highway construction purposes, (1992)

[18] SRPS EN 196-3 – Methods of testing cement – Part 3: Determination of setting times and soundness, (2017)

[19] SRPS EN 196-1 – Methods of testing cement – Part 1: Determination of strength, (2017)

[20] SRPS EN 14227-11 – Hydraulically bound mixtures – Specifications – Part 11: Soil treated by lime, (2013)

ORIGINAL SCIENTIFIC PAPER OPEN ACCESS

Measurement of motor vehicle speed as an input parameter in models for predicting noise levels

Žarko Đorđević[1*], Branko Radičević[2], Mišo Bjelić[2], Jovana Bojković[2]

[1] The Academy of Applied Technical Studies Šumadija, The Technical College of Applied Studies in Mechanical Engineering, Trstenik, Serbia

[2] University of Kragujevac, Faculty of Mechanical and Civil Engineering in Kraljevo, Serbia

ARTICLE INFO

* **Correspondence:** zaredj@gmail.com

DOI: 10.5937/engtoday2202045D

UDC: 621(497.11) **ISSN:** 2812-9474

Article history: Received 21 June 2022; Accepted 08 July 2022

ABSTRACT

Motor vehicle speed is one of the inputs used to develop models for predicting road traffic noise levels. In existing models, the vehicle speed used as input to estimate the noise level is not the current (measured) speed, but the vehicle speed determined based on the speed limit by road type or vehicle type. Therefore, the development of a device for measuring vehicle speed using radar that works on the principle of Doppler effect, which is presented in the paper. The advantage of this measuring device is the low price compared to similar devices, easy use and the possibility of easy processing of data obtained by measurement. The device allows measuring speed in all weather conditions in terms of temperature, precipitation and time of day. Then, in real time, it displays the speed and direction of movement of the vehicle on the screen of the mobile phone, and in the stationary laboratory, remote control, adjustment and adjustment of the software for measuring speed is enabled.

KEYWORDS

Noise level, Road traffic, Vehicle speed, Noise level predicting model

1. INTRODUCTION

Different models for predicting noise levels use speed to predict noise levels in different ways, so some of them are presented. Of course, it should be noted that in addition to these, there are other models that do not use the speed of the vehicle to predict noise levels.

1.1. CoRTN model

CoRTN model [1] [2] (Calculation of Road Traffic Noise) was developed in cooperation between TRRL (Transport and Road Research Laboratory) and the Ministry of Transport of the United Kingdom in 1975, and was modified in 1988. According to this model, the value of noise level generated by road traffic at a distance of 10 m from the closer edge of the road, which is exceeded during 10% (observed) of one-hour time interval can be estimated using the following equation (1):

$$L_{10}(1h) = 42{,}2 + 10\log Q + \Delta L_V + \Delta L_S + \Delta L_P + \Delta L_\alpha\ [dBA] \quad (1)$$

where:

Q – flow of motor vehicles (vehicles / hour),

ΔL_V – correction of noise levels for the impact of vehicle speed and the percentage of heavy vehicles,

ΔL_S – correction of noise levels to influence the slope of the road,

ΔL_P – correction of noise levels for the impact of the road curtain,

ΔL_α – correction of noise levels in the case of a line source of limited length.

An average speed of 75 km/h or a speed corresponding to the type of road is used to calculate the noise level.

1.2. RLS-90 model

RLS-90 model [1] [3] was developed by the Ministry of Transport (Road Construction Department) of the Federal Republic of Germany in 1990 to predict road traffic noise. This model establishes a connection between the parameters of traffic flow (vehicle flow, percentage of heavy vehicles, speed limit) and the average noise level at a distance of 25 m from the road axis. According to the RLS-90 model, the value of noise levels in the open space without vertical obstacles can be estimated as follows (2):

$$L_0 = 37{,}3 + 10 \log (Q\,(1 + 0{,}082p)) + \Delta L_V + \Delta L_S + \Delta L_P \; [dBA] \qquad (2)$$

Wherein:

Q – flow of motor vehicles (vehicles / time),

p – share of heavy vehicles in traffic flow (%),

ΔL_V – correction of noise levels for the impact of vehicle speed,

ΔL_S – correction of noise levels for the influence of road slope,

ΔL_P – correction of noise levels for the impact of the road curtain,

In this model, the speeds of passenger vehicles from 30 km/h to 130 km/h and the speeds of trucks from 30 km/h to 80 km/h are used to predict the noise of road vehicles.

1.3. Burgess model

This model [4] was developed at the National Physics Laboratory in Sydney. During the measurement, the traffic was free, on a flat road, without traffic signals. The analysis developed the equation for the equivalent noise level of road traffic and is presented as follows (3):

$$L_{eq} = 55 + 10.2 \log Q + 0.3p - 19.3 \log d \qquad (3)$$

Wherein:

Q – total number of vehicles,

p – share of heavy vehicles in traffic flow (%),

d – distance.

This model gives a satisfactory correlation value of 0.95 with a standard error of 1.5 dB compared to the measured Leq, noting that heavy vehicles greatly affect the noise level and that not taking into account the speed of the vehicle simplifies the model applies in uninterrupted traffic conditions in Australia.

1.4. ASJ RTN - model 2018

The model [4] [5] for predicting noise levels began to develop in the 1970s in Japan.

The model is based on certain conditions such as road type (pavement, road dimensions, signalized / non-signalized road sections), traffic volume, vehicle speed (interrupted / uninterrupted traffic flows), road length and meteorological conditions.

ASJ RTN-Model 2018 calculates noise levels of different vehicles depending on vehicle speed, engine speed and engine load, and the model is expressed as a function of vehicle speed, although the change in noise levels is due to the type of road and road slope and type and type vehicles. The noise level of road vehicles is calculated as follows (4):

$$L_{wA} = a + b \log V + C \qquad (4)$$

Wherein:

a, b – regression coefficient,

V – vehicle speed (km / h),

C – benchmark correction factor.

$C=\Delta L_{grad}+\Delta L_{dir}+\Delta Letc$

ΔL_{grad} is the correction for road gradient [dB],

ΔL_{dir} is the correction for sound radiation directivity [dB], and

ΔL_{etc} is the correction for other factors [dB]

provided that the model is especially used for sections with uninterrupted traffic flows (highways, motorways) with vehicle speeds of 40 to 140 km / h and for sections with interrupted traffic flows (intersections) with vehicle speeds of 10 to 60 km / h .

1.5. CNOSSOS model

In order to achieve a joint program to address environmental noise, the Council of Ministers of the European Union approved in 2002 Directive 2002/49 / EC on the assessment and management of environmental noise, which provides for a number of activities to implement measures that would contribute to avoiding, preventing or reducing the harmful effects of noise in the environment.

In accordance with Article 6.2 of Directive 2002/49 / EC, in 2012 the European Commission developed Common Noise Assessment Methods (CNOSSOS-EU) for road, rail and air transport, as well as industrial noise, which is applied in for the purpose of strategic noise mapping in accordance with Article 7 of the Directive, binding from 2019 in all EU countries.

CNOSSOS EU [6] aims to improve the reliability, consistency, and comparability of noise assessment results in EU Member States based on data from successive noise mapping cycles.

The source of road traffic noise is determined by combining the noise emissions of all individual vehicles that form the traffic flow. These vehicles are divided into five separate groups based on noise emission characteristics (1: light motor vehicles, 2: medium motor vehicles, 3: heavy motor vehicles, 4: two-wheeled motor vehicles and 5: open vehicle category

Each road vehicle emission model is represented by a set of mathematical equations that represent two main noise sources:

1. rolling noise, caused by the interaction of tires and road and
2. vehicle propulsion system noise (engine, exhaust system).

Rolling noise is defined by the equation (5):

$$L_{WR,i,m}=A_{R,i,m}+B_{R,i,m}log(\frac{v_m}{v_{ref}})+\Delta L_{WR,i,m} \tag{5}$$

Vehicle propulsion system noise is defined by the equation (6):

$$L_{WP,i,m}=A_{P,i,m}+B_{P,i,m}\left(\frac{v_m-v_{ref}}{v_{ref}}\right)+\Delta L_{WR,i,m} \tag{6}$$

Wherein:

$A_{P,i,m}$ and $B_{P,i,m}$ – octave band coefficients for each vehicle category,

v_{ref} - reference speed 70 km / h,

v_m - speed according to the type of vehicle (km/h),

$\Delta L_{WP,i,m}$ – speed according to vehicle type (km / h).

The coefficients $A_{P,\,i,\,m}$ and $B_{P,\,i,\,m}$ are given by octave bands for each vehicle category and for the reference speed v_{ref} = 70 km/h. ΔLWP, i, m is equal to the sum of the correction factors to be applied to the drive noise emission for special driving conditions or conditions other than the reference conditions.

vm represents speed according to the type of vehicle, with the definition that in most cases it is less than the speed limit according to the type of road and the highest speed according to the type of vehicle, assuming that all vehicles by category move at the same speed.

Based on the previously presented models for predicting road traffic noise, it can be seen that some models neglect vehicle speed due to model simplicity (Burgess model), some models such as CoRTN model and RLS-90 model use speed to correct noise levels, and ASJ RTN - the 2018 model and the CNOSSOS model use vehicle speed as one of the main factors for calculating noise levels.

2. CHARACTERISTICS OF SPEED MEASURING DEVICES

Some of the models that predict the noise level use the speed of the vehicle as one of the parameters. The speed used is usually not the current speed of the vehicle, but the speed that is defined on the basis of the speed limit for a certain type of road or for a certain type of vehicle on certain roads. An analysis of existing speed measurement systems has shown that their price is relatively high, that some are very difficult to use (eg speed radars used by the police), and that some of them cannot fully meet the required measurement requirements. speed.

In order to overcome the above problems, a speed measuring device was made. The speedometer consists of a radar, a camera, a mini PC housed in a housing, a power battery and a mobile phone. In the following text, the characteristics of individual elements of the speed measuring device will be presented.

2.1. Radar

The radar used in the speedometer is made by OmniPreSense model OPS243. The OmniPreSense OPS243 is a short-range radar that detects movement, measures speed and direction. The OPS243 block diagram of the radar is given in Figure 1.

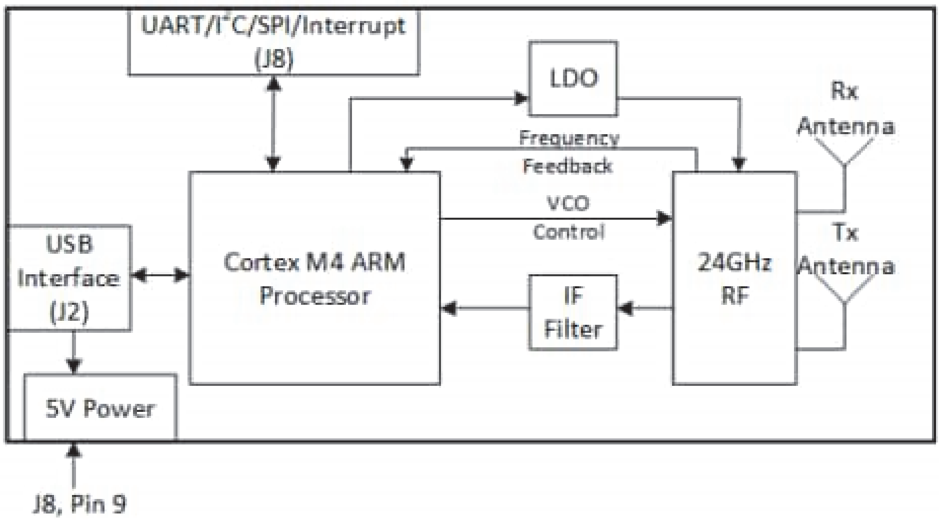

Figure 1: OPS243 radar block diagram

Radar signals are processed by an on-board processor which communicates via the API. The OPS243 communicates with the Raspberry Pi mini via a mini USB port. This radar detects (Figure 2) pedestrian-like objects at a distance of 25 m, large metal-like objects at a distance of up to 100 m, with a maximum speed of up to 222 km / h. The radar beam of measurement is 20o wide, consumption 1.7 W, in hibernation up to 0.2W and operating temperature from -40oC to +85oC.

Radar (Figure 3) works on the principle of Doppler effect, continuously sends fixed frequency radio waves that strike an object (vehicle) moving towards or from the radar. The frequency of the reflected radio wave is changed, and the speed of the moving object is obtained from the difference in frequency between the emitted and reflected radio waves.

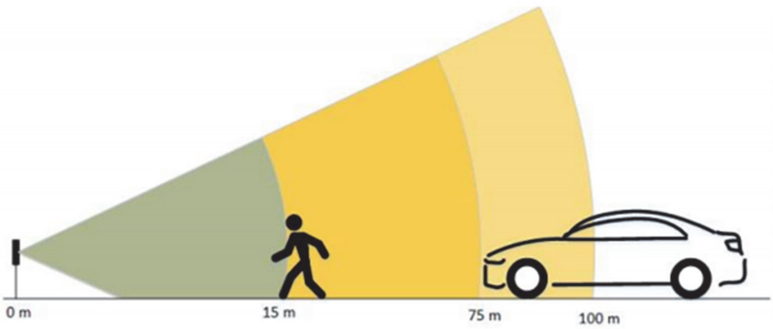

Figure 2: The distance at which moving objects are detected

If a radio wave is transmitted to a moving object moving away from the radar, each subsequent wave travels a greater distance to the object before it is reflected to the radar. Each subsequent wave travels longer, so the wavelength increases, while the frequency decreases. In case the radio wave is transmitted towards an object approaching the radar, each subsequent wave travels a smaller distance, so the wavelength decreases and the frequency increases.

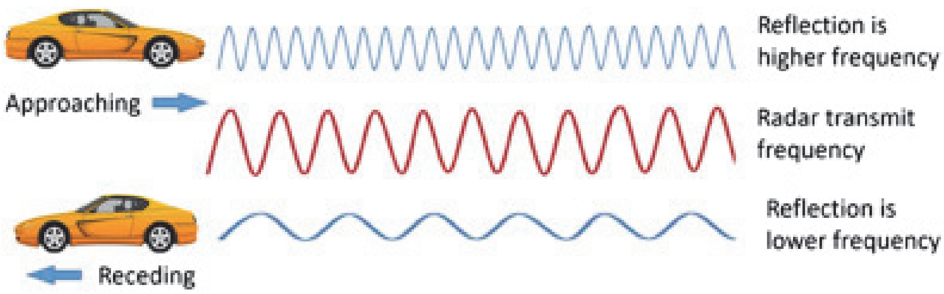

Figure 3: Principle of Doppler effect

2.2. Camera

Raspberry Pi V2 camera, uses Sony IMX219 8 mega pixel sensor. The camera is used to record videos and photos. It supports 1080p30, 720p60 and VGA90 video mode, connects via a 15 cm cable to the CSI port on a Raspberry Pi mini computer.

2.3. Mini PC

The Raspberry Pi 3 mini PC uses the Linux debian operating system. The Raspberry Pi 3 mini PC features a 64-bit quad-core 1.4GHz processor, 2.4GHz dual-band and 5GHz wireless LAN, Bluetooth 4.2 / BLE, faster Ethernet and PoE (Power over Ethernet). The mini PC is used in the unit for measuring speed due to its simple programmability.

Dedicated mini PC software downloads data from the radar API, collects photos taken with the camera and records the speed at the time of shooting. The device records the measured speed, at a certain magnitude of the reference signal, and the frequency of recording speed can be changed and adjusted via the API. Recorded data is stored on a micro SD card. All measurements are monitored over the network, and the mini PC is accessed from a web browser.

On the screen of the mobile phone, real-time video from the camera as well as the speed and direction of movement of the vehicle can be viewed via a web browser (it is not necessary to install any additional monitoring application on the phone). The mini PC computer accesses the hotspot via Wi-Fi (the hotspot function allows the Internet to be shared with other devices via mobile phones) activated on the mobile phone, thus enabling the mini PC to have internet access.

Since the Raspberry Pi 3 mini PC does not have a real-time clock on it, the correct time is set via the Internet. The mini computer makes a VPN connection to the stationary laboratory where the central computer is located, which enables the Raspberry Pi 3 computer to be accessed from the stationary laboratory in the field where the measurements are performed. In this way, remote control, adjustment and adjustment of speed measurement software is enabled. When measuring speed, the device can be set not to record a speed measured below a certain speed or only to record a speed measured above a certain speed.

3. RESULTS AND DISCUSSION

Figures 4, 5 and 6 give some of the possible views recorded by the speed measuring device. Figure 4 shows the measured speed (positive value) of the vehicle on arrival with the date (day.month.year) and time (hour: minute: second) when the speed measurement was performed, while Figure 5 shows the measured speed negative value) of the outgoing vehicle with the display of the date and time when the speed measurement was performed.

Figure 4. Recording the speed of movement vehicles; vehicle on arrival

Figure 6 shows all measured speeds by radar, ie more measured speeds per second, but the device is set to record one measured speed per second and this speed is shown in the image. This setting may be different, ie the device can record the speed several times per second, but for the type of measurements required, this is a satisfactory frequency of recording the measured speed.

Figure 5. Recording the speed of movement vehicles; outgoing vehicle

In order for the speed measuring device to have a practical application, it was calibrated with a laser radar TLaser III type B-1-32, serial number 110135 used by the Ministry of Interior of the Republic of Serbia, Traffic Police Administration and has a Certificate of verification valid until 30 June 2022. During the control measurement to check the correctness of the measurement, the speed measuring device showed identical results as the laser radar TLaser III, so it can be used during any speed measurement.

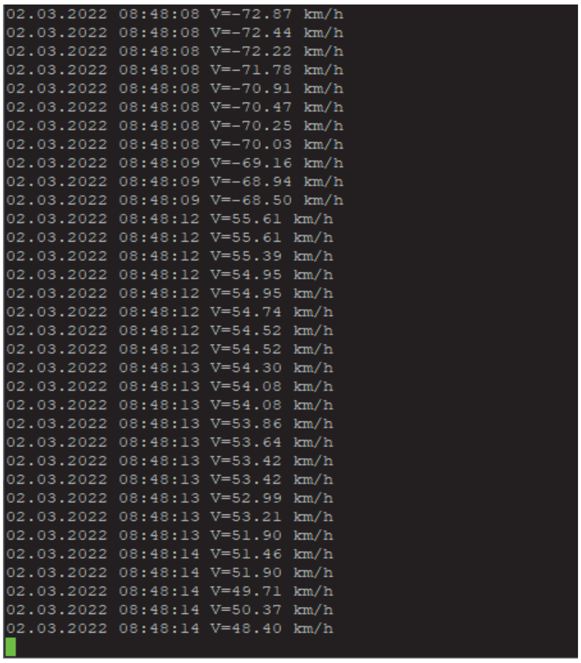

```
02.03.2022 08:48:08 V=-72.87 km/h
02.03.2022 08:48:08 V=-72.44 km/h
02.03.2022 08:48:08 V=-72.22 km/h
02.03.2022 08:48:08 V=-71.78 km/h
02.03.2022 08:48:08 V=-70.91 km/h
02.03.2022 08:48:08 V=-70.47 km/h
02.03.2022 08:48:08 V=-70.25 km/h
02.03.2022 08:48:08 V=-70.03 km/h
02.03.2022 08:48:09 V=-69.16 km/h
02.03.2022 08:48:09 V=-68.94 km/h
02.03.2022 08:48:09 V=-68.50 km/h
02.03.2022 08:48:12 V=55.61 km/h
02.03.2022 08:48:12 V=55.61 km/h
02.03.2022 08:48:12 V=55.39 km/h
02.03.2022 08:48:12 V=54.95 km/h
02.03.2022 08:48:12 V=54.95 km/h
02.03.2022 08:48:12 V=54.74 km/h
02.03.2022 08:48:12 V=54.52 km/h
02.03.2022 08:48:12 V=54.52 km/h
02.03.2022 08:48:13 V=54.30 km/h
02.03.2022 08:48:13 V=54.08 km/h
02.03.2022 08:48:13 V=54.08 km/h
02.03.2022 08:48:13 V=53.86 km/h
02.03.2022 08:48:13 V=53.64 km/h
02.03.2022 08:48:13 V=53.42 km/h
02.03.2022 08:48:13 V=53.42 km/h
02.03.2022 08:48:13 V=52.99 km/h
02.03.2022 08:48:13 V=53.21 km/h
02.03.2022 08:48:13 V=51.90 km/h
02.03.2022 08:48:14 V=51.46 km/h
02.03.2022 08:48:14 V=51.90 km/h
02.03.2022 08:48:14 V=49.71 km/h
02.03.2022 08:48:14 V=50.37 km/h
02.03.2022 08:48:14 V=48.40 km/h
```

Figure 6. Recording of all speeds from the radar

4. CONCLUSION

The measuring device performs stationary measurement and was primarily developed for measuring vehicle speed as one of the input parameters in the noise prediction model. In addition to this purpose, the measuring device can also be used for other vehicle speed measurements in order to record the vehicle speed on certain sections of the road. Further development of the measuring device aims at the device, in addition to measuring speed, also counting vehicles and recognizing the type of vehicle (motorcycles, passenger, cargo, etc.) in order to obtain the most accurate input data for predicting noise levels of road traffic. In addition to this, based on the measured values of speeds, it will be possible to form a model for planning road traffic noise for different values of vehicle speed, e.g. in the settlement, outside the settlement, motorway and highway.

5. LITERATURE

[1] J. Tomić, “Application of soft computing techniques for predicting road traffic noise levels”, PhD Thesis, University of Belgrade (Serbia), (2017)

[2] Department of Transport Welsh office, “Calculation of road traffic noise”, London, (England), (1988)

[3] Der Bundesminister für Verkehr, “Richtlinien für den Lärmschutz an Straßen RLS-90”, (1990)

[4] F. Ibili, E. K. Adanu, C. A. Adams, S. A. Andam-Akorful, S S. Turay and S. A. Ajayi, “Traffic noise models and noise guidelines: A review”, Noise & Vibration Worldwide 2021, Vol. 53 (1-2), pp. 65–79, https://doi.org/10.1177/09574565211052693, (2022)

[5] S. Sakamoto, “Road traffic noise prediction model ASJ RTN-Model 2018”, Acoust. Sci. & Tech., Vol. 41, (3), pp. 529-589, https://doi.org/10.1250/ast.41.529, (2020)

[6] S.Kephalopoulos, M. Paviotti, F. Anfosso-Lédée, “Common Noise Assessment Methods in Europe (CNOSSOS-EU)”, (2012)

ORIGINAL SCIENTIFIC PAPER OPEN ACCESS

Analysis of the performance of the shell and tube heat exchanger: influence of the baffles and the position of fluid inlet and outlet

Stefan Adžić[1], Nenad Stojić[1*], Miljan Marašević[1], Nebojša Bogojević[1], Jovana Bojković[1]

[1] University of Kragujevac, Faculty of Mechanical and Civil Engineering in Kraljevo, Serbia

ARTICLE INFO

[*] **Correspondence:** stojic.n@mfkv.kg.ac.rs

DOI: 10.5937/engtoday2202053A

UDC: 621(497.11) **ISSN:** 2812-9474

Article history: Received 17 June 2022; Accepted 12 July 2022

ABSTRACT

The constant need for heat exchangers that are easy to manufacture and maintain, and that have a standardized and already known manufacturing technology, has led to the fact that shell and tube heat exchangers are one of the most common devices used in the process industry. In this paper, the analytical and numerical models of the basic shell and heat exchanger have presented with dimensions of 3750 x 1000 mm and a nominal heat capacity of 410 kW. Using the flow simulation, the influence of different numbers and arrangement of baffles and the changing the position of the inlet and outlet of warmer fluid are considered. The temperatures of the fluids on the inlet and outlet are taken into account as the main parameters for heat exchanger performance. From obtained results, it can be concluded that with the increase in the number of baffles, the performance of the heat exchanger is increased. The position of the inlet and outlet of the warmer fluid greatly influence the heat exchanger performance.

KEYWORDS

Shell and tube heat exchanger, Simulation, Baffle

1. INTRODUCTION

Heat exchangers are devices in which heat is exchanged between warmer and colder fluids without a fluids mixture [1,2]. There are several groups and subgroups within the division of heat exchangers. The primary division of the heat exchanger is according to the purpose, temperature operating mode of the appliance, and functional-technical solutions. According to the purpose, heat exchangers can be used in industrial processes as heaters and coolers, evaporators and crystallizers, evaporators and condensers, and chemical and biochemical reactors, while the division according to the operating temperature is divided into a low temperature, medium temperature, high temperature, and cryogenic heat exchangers. The most common division of heat exchangers is according to the method of heat transfer from one fluid to another, and this classification was made according to functional-technological solutions. According to the method of heat transfer, we distinguish: regenerative exchangers, recuperative exchangers, exchangers with indirect heat carriers, and contact heat exchangers. Geometric characteristics affect the change in heat flux, primarily by changing the velocity and current flow of the fluid, which makes the geometric characteristics an important parameter when choosing a model of the shell and tube heat exchanger. Experimental examination of different design studies of the heat exchangers requires a lot of time, therefore simulation studies are usually used for the analysis of the influence of parameters on the heat exchanger performance [3]. Bicer et al [4] analyzed the influence of the different baffle designs to reduce the pressure drop and increase the efficiency of the heat exchanger. In their paper, the Taguchi method was used to determine the optimal design of baffles solution. The proposed design leads to a 7.3% increase in the heat transfer rate and a 7.6% pressure drop. Safarian at all [3] considered the influence of the elliptical tube cross-sections on the pressure drop and heat transfer coefficient of the heat exchanger. Abd et al [5] investigate the influence of the shell diameter and tube length on the heat transfer coefficient and pressure drop. Heat transfer coefficient and pressure drop will decrease with increasing the space between the baffles. Increasing the shell diameter, the pressure drop will decrease while an increase in the tube length leads to enhancing the heat transfer coefficient and pressure drop. Labbadlia et al [6] have shown that tube arrangements in the shell and tube heat exchanger have a significant influence on the efficiency. They were investigating four different tube arrangements and show that is possible to achieve better flow distribution as well as better pressure distribution uniformity. Innovative steps in the industry contribute to obtaining better optimization solutions when designing the construction of heat exchangers. The main priority when designing the construction of the heat exchanger is the tendency towards the smallest possible dimension of the device and the highest possible efficiency of the exchanger. Good geometric characteristics achieve more intensive heat exchange between fluids without increasing the size and weight of the device, which affects the manufacturing cost of the heat exchanger.

The paper presents an analysis of three variant solutions for optimizing the construction of a shell and tube heat exchanger by changing the arrangement and number of baffles and changing the position of the warmer fluid inlet and outlet. Before the simulation and analysis of the basic model of the exchanger, the geometrical characteristics, mass flows of the fluid, inlet and outlet temperatures of fluid 1 (warmer fluid-water) and fluid 2 (colder fluid-water) were determined. The length of the active part of the appliance is 3750 mm, the diameter of the appliance is 1000 mm, the number of pipes in the pipe register is 81 and they are arranged to correspond to the circular arrangement, as shown in Figure 1. Based on the input parameters, the rated power of the basic model of the heat exchanger is 410 kW. During the simulation of the operation of the shell and tube heat exchanger, uneven fluid flow and low outlet temperature of the colder fluid were observed. In the continuation of the paper, three optimization geometric solutions are presented, which aim to achieve a more uniform fluid flow and as high an output temperature of the colder fluid as possible. The basic geometric characteristics and input parameters of the fluid are the same in all optimization solutions. [7], [8].

2. SHELL AND TUBE HEAT EXCHANGER

Shell and tube heat exchangers are a type of recuperative heat exchangers and have a wide representation in the process industry [1,8,9]. They have been used for more than 14 decades, while in the last few decades they have appeared as standardized and standardized constructions. One of the most well-known standardized constructions is, according to the TEMA standard, within the framework of the American Tubular Exchanger Manufacturers Association (TEMA). The shell and tube heat exchanger can be of robust construction, the surface of the heat exchanger can be up to 5000 m2, while the length of the heat exchanger can reach up to 12 m. The maximum temperature difference between the pipe register and the shell is from 20 ˚C to 600 ˚C. Due to their high rigidity, they are suitable for operation at high pressures and in a vacuum. Shell and tube heat exchangers have two basic parts, one of which is the inner part which consists of a pipe register, and the outer part which consists of the shell, the front and the rear head. During construction and construction solutions, it is possible that the inner and outer parts can be separated. The front head on the shell and tube heat exchanger is always fixed, while the rear head can be positioned so that it is fixed or floating. The liquid that is introduced into the apparatus can achieve its flow along the pipe or at the same time along and transversely on the pipe if baffles are placed. Baffles on the shell and tube heat exchanger theoretically represent external elements but are often placed in the pipe register. The connection of the pipe to the pipe plate in a shell and tube heat exchanger is usually achieved by welding. The fluid flowing through the pipes has an inlet and outlet connection on the heads, while the fluid flowing around the pipe has its connections on the exchanger shell itself, Fig. 1.

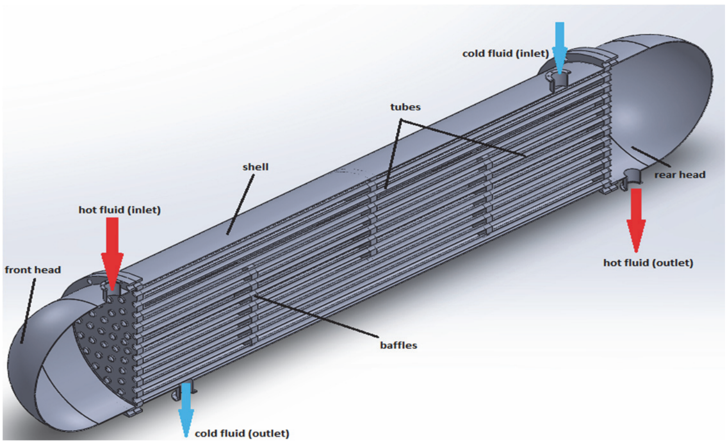

Figure 1: The basic construction of the shell and tube heat exchanger

Several important rules determine the distribution of fluid in a shell and tube heat exchanger. Fluids of higher pressure in most cases flow through a pipe. Small pipe diameters and nominal wall thickness withstand high pressures more easily and give a lower construction cost. Also, the fluid with a higher coefficient of contamination should be placed in the pipe register because the pipes are easier to clean by mechanical methods. Since water is used in the simulation for both fluids in the tubular exchanger, the main reason for adopting this fluid position is flow analysis, i.e. fluid with the lower flow is more adequately placed in the tubular register because it enables greater heat transfer from the register tube (increase in flow rate). [7]

3. MODELING AND CALCULATION

When creating a model of the exchanger, it is necessary to perform calculations of the amount of heat exchanged between two fluids, taking into account the following parameters: mass flow, inlet temperatures of both fluids, and outlet temperature of one of the fluids. The energy balance of a heat exchanger is determined from the equation:

$$Q=\dot{m}_1\cdot c_{p1}\cdot\left(t_{1\,in}-t_{1\,out}\right)=\dot{m}_2\cdot c_{p2}\cdot\left(t_{2\,out}-t_{2\,in}\right)=k\cdot A_{exch}\cdot\Delta t_m \tag{1}$$

where are: $\dot{m}_1$ - mass flow rate of the fluid 1, $c_{p,1}$ -specific heat capacity of the fluid 1, $t_{1\,in}$ - inlet temperature of the fluid 1, t_{1out} - outlet temperature of the fluid 1, $\dot{m}_2$ -mass flow rate of the fluid 2, c_{p2} - specific heat capacity of the fluid 2, $t_{2\,in}$ - inlet temperature of the fluid 2, t_{2out} - outlet temperature of the fluid 2.

The mean logarithmic temperature difference is determined from equation (2) for a heat exchanger with counterflow, taking into account correction factor ε taken from [9, 10,11]:

$$\Delta t_{mlog}=\varepsilon\cdot\frac{\left(t_{1\,in}-t_{2\,out}\right)-\left(t_{1\,out}-t_{2\,in}\right)}{ln\left(\dfrac{t_{1\,in}-t_{2\,out}}{t_{1\,out}-t_{2\,in}}\right)} \tag{2}$$

Based on the known geometry of the shell and tube heat exchanger on the basis of the known inlet and outlet temperature of both fluids obtained from (1), the heat transfer coefficient is calculated:

$$k=\frac{1}{\left(\dfrac{1}{\alpha_1}+R_{f1}\right)\dfrac{A_2}{A_1}+R_{wall}+\dfrac{1}{\alpha_2}+R_{f2}} \tag{3}$$

where: α_i-heat transfer coefficients, A_i-heat transfer areas, R_{f1} - fouling resistances, R_{wall} -thermal resistance of the separating wall. [12]

The heat resistance coefficients due to contamination were adopted from [11]:

$$R_{f1}=0{,}2\cdot10^{-3}\,\frac{m^2K}{W}\quad\text{and}\quad R_{f2}=0{,}1\cdot10^{-3}\,\frac{m^2K}{W} \tag{4}$$

Convective heat transfer coefficient is obtained by the formula:

$$\alpha_i=\frac{Nu_i\cdot\lambda_i}{d_{e,i}} \tag{5}$$

where are: λ_i – the coefficient of the conduction, $d_{e,i}$ – the equivalent diameter, Nu_i – Nusselt number [8].

Dimensionless numbers, required for determination of the heat transfer coefficient, were calculated from (6) and (7).

$$Nu_i=0{,}21\cdot\mathrm{Re}_i^{0{,}6}\cdot Pr_i^{\frac{1}{3}} \tag{6}$$

$$\mathrm{Re}_i=\frac{w_i\cdot d_{e,i}\cdot\rho_i}{\mu_i} \tag{7}$$

where are: w_i – the fluid velocity, ρ_i – the fluid density, μ_i – the coefficient of dynamic viscosity of the fluids, Re_i – Reynolds number, Pr_i – Prandtl number, where is $i=1$ - for fluid 1, $i=2$ – for fluid 2.

Based on previous, the outlet temperature of the fluids and heat transfer coefficient were determined for the given input parameters. The specific heat capacities of both fluids were adopted based on the mean temperatures from [9, 10, 11].

Table 1: Parameters of the basic design of shell and tube heat exchanger obtained by analytical calculations

$\dot{m}_1$ [kg/s]	$t_{1\,in}$ [°C]	$t_{1\,out}$ [°C]	c_{p1} [kJ/kg°C]	Δt_m [°C]
1,67	180	123	4,3075	94,11
$\dot{m}_2$ [kg/s]	$t_{2\,in}$ [°C]	$t_{2\,out}$ [°C]	c_{p2} [kJ/kg°C]	k [W/m²K]
2,9	40	73.8	4,1833	118,89

4. MODEL VALIDATION

Validation of the numerical model was performed by comparison of the results obtained from analytical calculations and results from flow simulations for the basic construction of the shell and tube heat exchanger. The mass flow of the fluids, the inlet temperatures of the both fluids are the same in analytical and flow analysis. The outlet temperature of the colder fluid was the parameter that was used for model validation. The temperature obtained from analytical model was 73.8 °C, while the temperature from flow simulation was 70.57 °C. Regarding that difference between the temperatures on the outlet of the colder fluid is 4.4% the simulation model is able to predict the temperature exchange in the heat exchanger.

5. FLOW ANALYSIS USING SOLIDWORKS FLOW SIMULATION

Using the known input parameters and geometrical characteristics of the exchanger, a simulation of fluid flow in the shell and tube heat exchanger, which is the basic model of the exchanger and on which the analysis will be performed. Fluid flow simulation of the basic model of the heat exchanger has shown uneven fluid flow during operation, which was the main reason for further analysis of the heat exchanger efficiency. For all proposed designs of the heater exchanger, the following parameters were taken into account: the system is adiabatically isolated, fluid flow is countercurrent, fluids entering the apparatus have a fully developed flow, heat exchanger is made of steel, number of inlets and outlets for warmer and the colder fluid is the same in all variant solutions. Fluid flow simulation in the basic model of the heat exchanger and the shown temperature fields indicate an uneven fluid flow in the tubular register of the exchanger. The cause of uneven fluid flow is the inadequate position of the inlet and outlet openings of the warmer fluid, as well as the layout and number of baffles within the pipe register, as shown in Fig. 2.

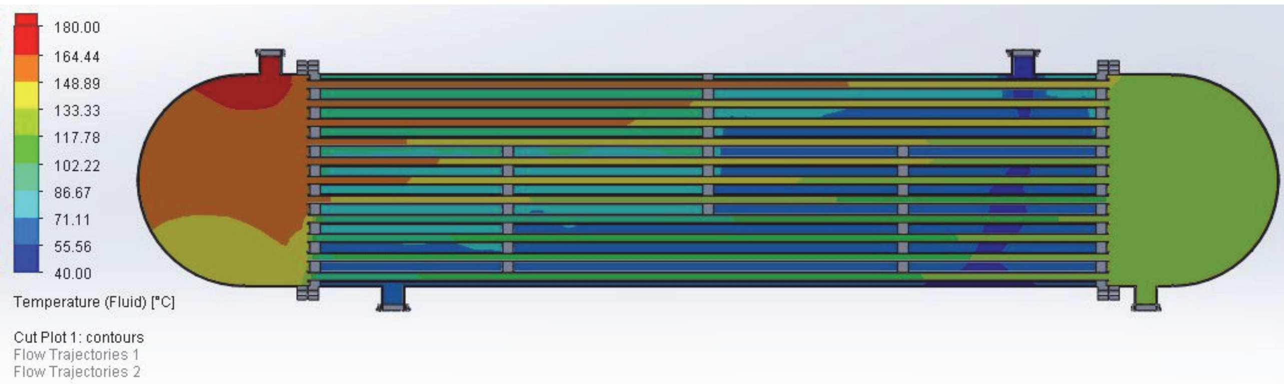

Figure 2: Temperature field for the basic model of shell and tube heat exchanger obtained by simulation

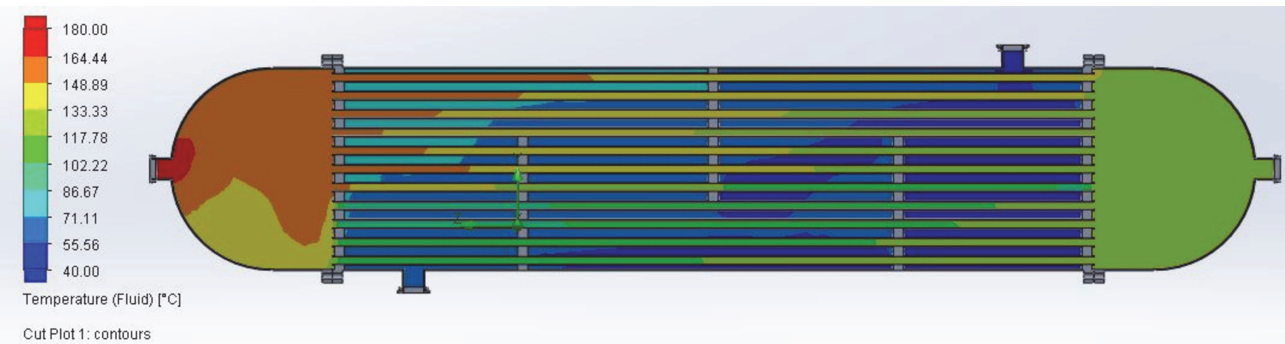

Figure 3: Temperature field for the model with the change of position of warmer fluid inlet and outlet obtained by simulation

In order to increase the effectiveness of the heat exchanger, i.e., in order to transfer as much heat between the two fluids as possible, it is necessary to optimize the geometric characteristics of the heat exchanger. Fluid inlets and outlets have a connection located on the exchanger heads. Changing the position of the inlet and outlet of the warmer fluid allows a more adequate and entry of fluid into the pipe register with higher velocity. Analysis of fluid flow simulation when changing the position of the inlet and outlet of the warmer shows that in addition to more adequate inlet and outlet of fluid from the pipe register, it is necessary to change the geometric structures related to the layout and number of baffles. The disadvantage of a variant solution in optimizations that involves changing the position of the inlet and outlet of the warmer fluid without additional optimization solutions is insufficient long retention of the warmer fluid through the pipe register and uneven flow that reduces heat exchange between the two fluids, as shown in Figure 3.

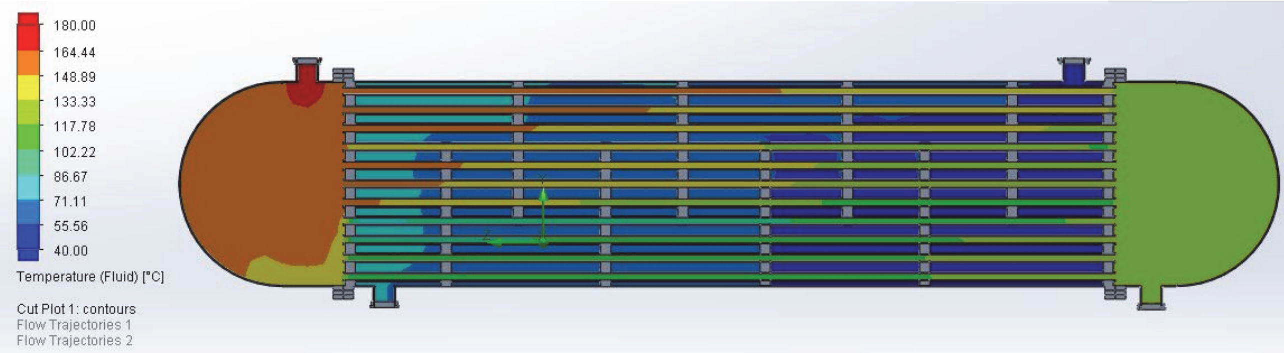

Figure 4: Temperature field for the model with changed number and layout of baffles obtained by simulation

In order to achieve the most even flow of fluid in the pipe register, the number and arrangement of baffles were optimized. In addition to the existing number baffles, optimization was performed and the number of baffles in the pipe register was increased. The variant solution includes the installation of a total of 8 baffles with equal lengths and distances, as shown in Figure 4. The increase in the number of baffles resulted in a more uniform fluid flow in the cervical register and a greater heat exchange between the warmer and colder fluids. By simulating the fluid flow when applying this variant of the solution, the results were obtained which show that by increasing the number of baffles, a higher outlet temperature of the colder fluid and thus a larger temperature difference is obtained.

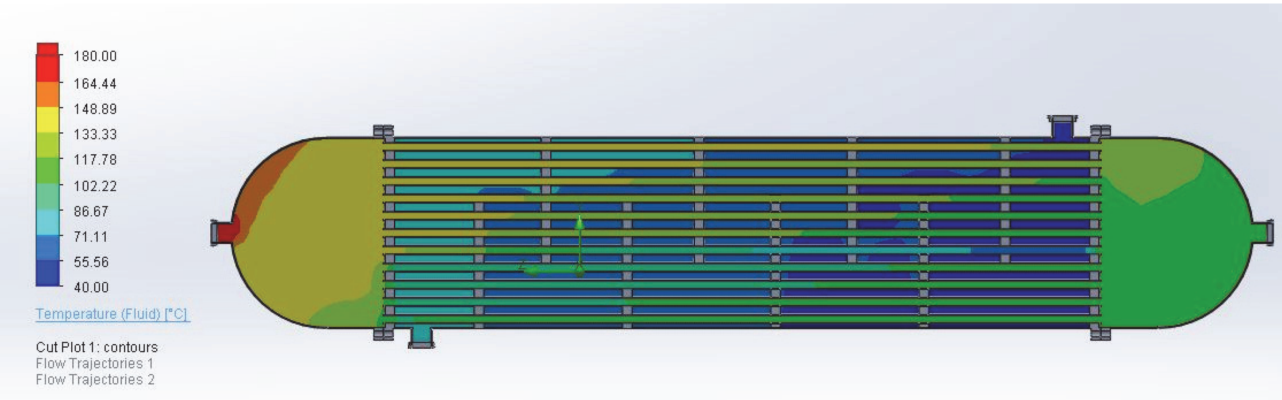

Figure 5: Temperature field for the model with changed the number and layout of baffles and position of warmer fluid inlet and outlet obtained by simulation

Despite the optimization solution that includes changing the layout and number of baffles, analyzes of fluid flow simulation and temperature fields show that the flow of warmer fluid in the pipe register can still be improved. For greater heat exchange, it is necessary to apply optimization solutions which, in addition to changing the layout and number of l baffles, also include changing the position of the warmer fluid inlet and outlet, as shown in Figure 5. The optimization solution, which includes a change in the layout and number of baffles, as well as a change in the position of the warmer fluid inlet and outlet, achieves a uniform fluid flow and a more adequate entry of the warmer fluid into the pipe register.

6. RESULTS AND ANALYSIS

The following table shows the values of fluid inlet and outlet temperatures in the simulation of the operation of shell and tube heat exchanger in which three optimization geometry solutions were made. Based on the simulation and analysis of fluid flow, it is concluded that the most adequate optimization solution is the one in which the largest temperature difference is obtained. In all optimization solutions, the values of the mass flows of colder and warmer fluids did not change, as did the inlet temperatures of the fluid. Therefore, by increasing the number of baffles and changing the position of the warmer inlet and outlet, the most uniform flow in the pipe register is achieved, that is, this variant solution achieves the greatest heat exchange between the colder and warmer fluid.

Table 2: Inlet and outlet temperatures depending of type construction obtained by simulation

Fluid	**Fluid 1 - water (warmer)**		**Fluid 2 - water (colder)**	
Temperature	t_{1in} [°C]	t_{1out} [°C]	t_{2in} [°C]	t_{2out} [°C]
Basic design	180	120,30	40	70,57
Basic design with changing the position of the warmer fluid inlet and outlet	180	126,40	40	67,67
Basic design with eight baffles	180	123,47	40	71,38
Basic design with eight baffles and changed the position of the warmer fluid inlet and outlet	**180**	**115,76**	**40**	**74,31**

Bearing in mind the same values of the inlet temperature of the colder and warmer fluid in all variant cases, we conclude that the amount of heat exchanged in the exchanger depends on the temperature differences. The table shows the values of the inlet and outlet temperatures of the hotter and colder fluid in all variant solutions. The outlet temperatures of the colder and warmer fluid depend on the application of the optimization solution of the geometric characteristics.

Effectiveness ε is a measure of thermal performance of a heat exchanger. It is defined for a given heat exchanger of any flow arrangement as a ratio of the actual heat transfer rate from the hot fluid to the cold fluid to the maximum possible heat transfer rate q_{max} thermodynamically permitted:

$$\varepsilon = \frac{q}{q_{max}} \tag{8}$$

where: q -total or local heat transfer rate in the exchanger, q_{max} - thermodynamically maximum possible heat transfer rate in a counterflow heat exchanger.

An overall energy balance for the two fluid streams is [13]:

$$q = C_h \cdot \left(t_{1,in} - t_{1out}\right) = C_c \cdot \left(t_{2,out} - t_{2in}\right) \tag{9}$$

$$q_{max} = C_{p1} \cdot \left(t_{1,in} - t_{2in}\right) = C_{p1} \cdot \Delta t_{max} \tag{10}$$

where: $C_h = m_1 \cdot c_{p1}$ - hot fluid capacity rate, and $C_c = m_2 \cdot c_{p2}$ - cold fluid capacity rate.

Table 3: Effectiveness of the analyzed designs of the heat exchanger

Effectiveness [%]			
Basic design	Basic design with changing the position of the fluid inlet and outlet	Basic design with eight baffles	Basic design with eight baffles and changing the position of the fluid inlet and outlet
36.82	33.26	37.76	41.39

7. CONCLUSION

The paper presents the analysis of geometric characteristics in the operation of shell and tube heat exchanger with two floating heads. Fluid flow simulation of the basic model of the heat exchanger with the required input parameters was performed. Based on the obtained results, the design of the exchanger was improved in order to achieve higher heat exchange between the two fluids. Simulations were performed in the software package "Solidworks" for three variant solutions. Higher heat exchange between the two fluids was achieved by the adjusting the number of the baffles and changing the position of the wormer fluid inlet and outlet, which gave a more uniform fluid flow in the exchanger. The nominal heat flux of the heat exchanger before the improvement was 410 kW. By applying the proposed design, for the same input parameters, the nominal heat flux of the heat exchanger has increased and reach 465 kW, which represents an increase of heat exchange between fluids for more than 13%.

The effectiveness of the proposed design solution has been calculated and increase of the 4.57 % achieved in the case of the heat exchanger with eight baffles and revised position of the warmer fluid inlet and outlet.

Proposed design solution would include the installation baffles and change of the position of the inlet and outlet of the warmer fluid, which will not have effect on the manufacturing costs of the heat exchanger. The proposed design has retained the dimensions of the basic heat exchanger, also the arrangements of the tube register have no changes as well as tubes length.

ACKNOWLEDGMENT

This research has been supported by the Serbian Ministry of the Education, Science and Technology Development under grant 451-03-68/2022-14/200108.

REFERENCES

[1] S. H. Gawande, S. D. Wankhede, R. N. Yerrawar, V. J. Sonawane and U. B. Ubarhande, “Design and Development of Shell & Tube Heat Exchanger for Beverage”, Modern Mechanical Engineering Vol. 2 No. 4, p.121, https://doi.org/10.4236/mme.2012.24015, (2012)

[2] Liang-YuChen, V. S. K. Adi and R. Laxmidewi, “Shell and tube heat exchanger flexible design strategy for process operability”, Case Studies in Thermal Engineering, 102163, https://doi.org/10.1016/j.csite.2022.102163

[3] M. R. Safarian, F. Fazelpou and M. Sham, “Numerical study of shell and tube heat exchanger with diferent cross-section tubes and combined tubes”, nternational Journal of Energy and Environmental Engineering,Vol. 10, pp. 33–46, https://doi.org/10.1007/s40095-019-0297-9, (2019)

[4] N. Biçer, T. Engin, H. Yas¸ E. Büyükkaya, A. Aydın and A. Topuz, “Design optimization of a shell-and-tube heat exchanger with novel three-zonal baffle by using CFD and taguchi method”, International Journal of Thermal Sciences, Vol. 155, p. 106417, https://doi.org/10.1016/j.ijthermalsci.2020.106417, (2020)

[5] A. A. Abd, M. Q. Kareem and S. Z. Naji, “Performance analysis of shell and tube heat exchanger: Parametric study”, Case Studies in Thermal Engineering, Vol. 12, pp. 563-568, https://doi.org/10.1016/j.csite.2018.07.009, (2018)

[6] O. Labbadlia, B. Laribi, B. Chetti and P. Hendrick, ”Numerical study of the influence of tube arrangement on the flow distribution in the header of shell and tube heat exchangers” Appl. Therm. Eng, Vol. 126, pp. 315–321, https://doi.org/10.1016/j.applthermaleng.2017.07.184, (2017)

[7] M. Rikalović, Dobošasti razmenjivači toplote, Savez mašinskih i elektrotehničkin inženjera i tehničara Srbije, Beograd (2002)

[8] M. Marašević, N. Bogojević, N. Stojić, S. Adžić and D.Šimunović, “Optimization of compact heat exchanger ”, Proceedings of X International Conference “Heavy Machinery HM 2021”, Vrnjačka Banja (Serbia), 22 June 25 June 2021, pp. 497-502, (2021)

[9] B. Jaćimović, S. Genić, Toplotne operacije i aparati – Deo 1: Rekuperativni razmenjivači toplote, Mašinski fakultet, Beograd, (2016)

[10] S. Genić, B. Jaćimović, M. Jarić and N. Budimir, Svojstva procesnih fluida, Savez mašinskih i elektrotehničkih inženjera i tehničara Srbije, Beograd, (2014)

[11] B. Jaćimović, S. Genić, M. Nagi and J. Laza, Problemi iz toplotnih operacija i aparata, SMEITS i Mašinski fakultet, Beograd, (1996)

[12] VDI Heat Atlas, C4 Fouling of Heat Exchanger Surfaces, Springer-Verlag Berlin Heidelberg, https://doi.org/10.1007/978-3-540-77877-6_7, (2010)

[13] R. K. Shah and D. P. Sekulić, Fundamentals of Heat Exchanger Design. John Wiley & Sons, Inc, https://doi.org/10.1002/9780470172605, (2003)

Engineering
TODAY

VOL. 1 / NO. 2/ 2022

CONTENTS